FROM MAGMATIC TO METAMORPHIC DEFORMATIONS IN A JURASSIC OPHIOLITIC COMPLEX: THE BRACCO GABBROIC MASSIF, EASTERN LIGURIA (ITALY)

Francesco Menna*,✉

* *Department of Earth Sciences, University of Florence, Italy.*
✉ *Corresponding author, e-mail: francesco.menna@unifi.it; francesco.menna77@gmail.com*

Keywords: *ophiolites, gabbro, HT-shear zones. Northern Apennines, Italy.*

ABSTRACT

A new structural study with multiscale detailed analysis of the main elements of the fabric was performed on the Bracco ophiolitic massif (Eastern Liguria). The results are here presented with a reconstruction of the sequence of events which characterized the evolution of the gabbroic complex, starting form the first magmatic phases up to the late metamorphic ones, through a retrograde path which ended with the final exposure of the gabbro on the ocean floor.

The field observations, supported by petrographic analyses, lead to outline for the Bracco Gabbroic Complex a deformative evolution which started in the early magmatic phases; the study of the metamorphic structures, following the intrusion and the syn-magmatic deformation of the gabbroic complex, allowed to identify three distinct metamorphic phases, whose petrographic features show that the associated deformations could actually represent a continuous evolution of the same tectonic phenomenon, which started under granulitic facies conditions, continued in amphibolitic facies and ended with deformations and recrystallizations in greenschist facies conditions.

INTRODUCTION

Geological studies on ophiolitic successions allow to observe continuously, in the field, lithologic and structural features linked to the formation and to the evolution of old oceanic crust, and to obtain all the informations collected along the present-day ridge systems, only with limited point sampling during oceanographic expeditions (e.g., *Ocean Drilling Program*-ODP, *Integrated Ocean Drilling Program*-IODP).

Being characterized only by a weak orogenic metamorphic imprint (Garuti et al., 2009), the ophiolites of the Northern Apennines (Fig. 1) preserve primary mineralogic-petrographic and structural features, better than other peri-Mediterranean ophiolitic successions. Therefore, a structural and petrographic study on these rocks allows to discriminate between oceanic and orogenic deformations and to acquire data on the metamorphic/deformative phases, connected to the Jurassic oceanic opening stage.

The Bracco ophiolitic massif (Eastern Liguria) represents one of the largest and better exposed ophiolitic successions in the Northern Apennines (Fig. 1). Starting from the late ’60, many geological and mineralogic-petrographic studies focused on the ophiolites of the Northern Apennines (Passerini, 1965; Abbate and Sagri, 1970; Bezzi and Piccardo, 1971; Decandia and Elter, 1972; Gianelli and Principi, 1974; Cortesogno et al., 1975). Nevertheless, precise structural studies on these successions started being published only from the end of the ’80 (Cortesogno et al., 1987; Hoogerduijn-Strating, 1988; 1991; Molli, 1992; 1994; 1995; 1996; Hoogerduijn-Strating et al., 1993; Treves and Harper, 1994).

This paper shows the results of a new detailed structural study, carried out on the Bracco ophiolitic massif that focused at outlining, at all the scales, the main elements of the fabric and at reconstructing the sequence of deformation events which led to the evolution of the Bracco Gabbroic Complex (BGC), starting form the first magmatic phases up to the late metamorphic ones, through a retrograde path which ended with the final exposure of the gabbro on the ocean floor. The study of the geometric relations and orientations of structures can shed light on the tectonic regime that was active on the Ligurian sector of the Western Tethys Ocean.

GEOLOGICAL SETTING AND PETROGRAPHY

The study area (Fig. 2) is characterized by the tectonic superimposition of three units: two belong to the Ligurian Domain, the Gottero Unit and the Bracco-Val Graveglia Unit, and one to the Sub-Ligurian Domain, the Canetolo Unit. The Gottero Unit is the highest in the structural pile and lies onto the Bracco-Val Graveglia Unit, thrust onto the Canetolo Unit.

The Bracco-Val Graveglia tectonic Unit as a whole represents a complete ophiolitic sequence, made of a basement and a volcano-sedimentary complex, followed by a pelagic cover (Fig. 3). Often described as a single ophiolitic sequence, it is actually formed by a quite complex set of tectonic slices, showing similar lito-stratigraphic features and common relationships among the formations. In particular, the Bracco-Val Graveglia Unit can be divided into three tectonic sub-units (Fig. 2): the Velva Sub-Unit at the top, formed in turn (Cortesogno et al., 1987) by the Monte Rossola (thick volcano-sedimentary successions) and Mezzema Elements (lerzholitic peridotites and cover formations), the San Nicolao Sub-Unit, corresponding to the gabbroic complex *s.s.* (Mezzama Element in Cortesogno et al., 1987) and the Pavereto Sub-Unit at the base (cover sequences, locally associated to tectonic slices of serpentinites and lherzolites). The ophiolitic basement is formed by lherzolitic peridotites (Cortesogno et al., 1987; Rampone et al., 1993; Piccardo et al., 1994) extensively intruded by a gabbroic complex, including local intercalations of plagioclase peridotites and/or dunites, which represent the femic differentiates of the gabbro (Cortesogno et al., 1987). This ‘ensemble’ is cross-cut by basalt dykes (MORB affinity: Cortesogno and Gaggero, 1992, and references therein), repre-

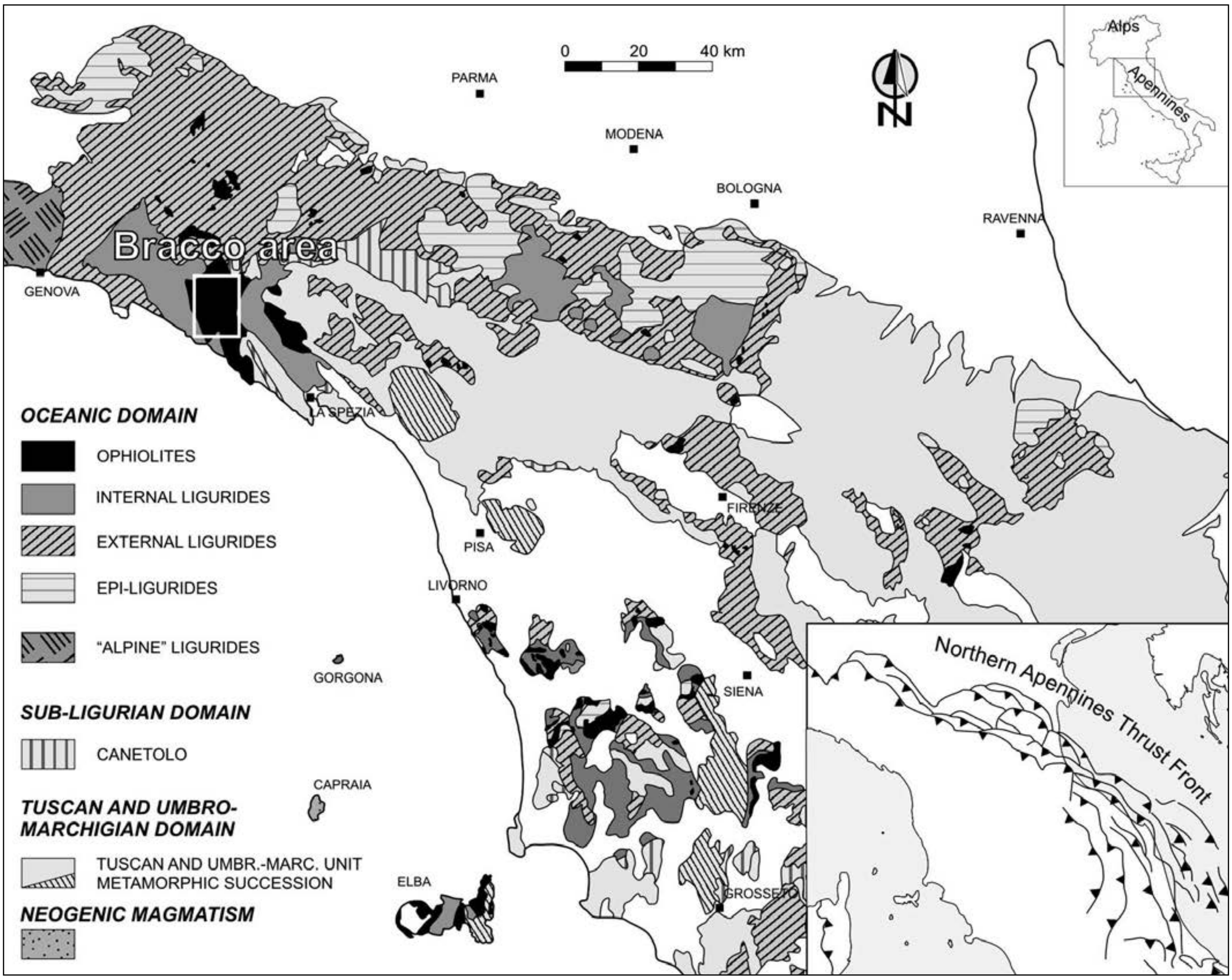

Fig. 1 - Schematic geological map of the Northern Apennines with location of the study area (modified after Principi et al., 2004).

senting the last magmatic event involving the basement, before its exposure on the ocean floor.

Lherzolitic peridotites

The lherzolitic peridotites appear in the field as massive rocks, dark bluish green to black in colour at the fresh cut, with a beige-light brown alteration coat. A "tectonitic" foliation, marked by the alignment of pyroxenes, is frequently visible (Fig. 4): pyroxenitic bands may be sometimes present, marking discrete levels with different compositions, generally parallel to the foliation.

Serpentinization phenomena determine a diffuse recrystallization of the rock, mainly at the expenses of olivine and orthopyroxene; clinopyroxene and spinel are instead better preserved. The orthopyroxene crystals, generally represented by pseudomorphic bastite (Cottin, 1978), often preserve the original habitus and may reach 10-15 mm in dimension. They are frequently characterized by exsolution lamellae of clinopyroxene, arranged along the cleavage planes. Analogously, in the clinopyroxene phenocrysts exsolution lamellae of orthopyroxene, often substituted by chlorite, are observed. Olivine crystals are rarely visible, forming mainly little fragments in the "mesh structure" of serpentine. Based on the pseudomorphosis textures (Cortesogno et al., 1987), we could reconstruct a protolith mainly formed by olivine (50%), orthopyroxene (10-30%), clinopyorxene (0-20%), red-brown chromite or green aluminium spinel (< 4%). In the volumes of rock characterized by tectonitic texture, the orthopyroxene is intensely deformed (microfolds and undulose extinction) and/or recrystallized in granoblastic aggregates. The age of the protolith can be referred to the Proterozoic (Rampone and Piccardo, 2000), while the tectonitic foliation, based on the analogy with the peridotites found in the External Ligurides (Beccaluva et al., 1984; Piccardo et al., 1990; Rampone et al., 1993; Rampone and Piccardo, 2000), can be attributed to the Permian and the serpentinization event to the Middle-Late Jurassic (Cortesogno et al., 1987). The thickness of these masses is difficult to estimate, since they form isolated bodies inside the gabbroic complex. In the areas where the largest bodies crop out (i.e., Moggia and Canegreca), the assessed thickness exceeds 100 m. In the neighbouring zones, outside the studied area (e.g., Monte Rossola), the maximum thickness reaches 250 m.

The contacts between the gabbros and the other lithotypes are generally tectonic; in the rare cases of preserved primary contacts, the gabbro may form dykes in the peridotite mass or is enclosed as lenses. The contacts with the main gabbroic complex (San Nicolao Sub-Unit) are generally represented by sharp surfaces; strips of lherzolites may locally be present inside the gabbro as well. Structures such as "*chilled margins*" have never been observed in the gabbro. Inside the dykes a magmatic foliation parallel to the borders can be sometimes observed (e.g., C. Canne locality, near Passano). The lherzolite-gabbro interface may be at times characterized by the presence of pyroxenitic levels (Cortesogno et al., 1987).

Bracco Gabbroic Complex (BGC)

It comprises both the magmatic complex and the olivine and/or pyroxene gabbros (Sm/Nd age of 164±14 My according to Rampone and Piccardo, 2000) with their femic differ-

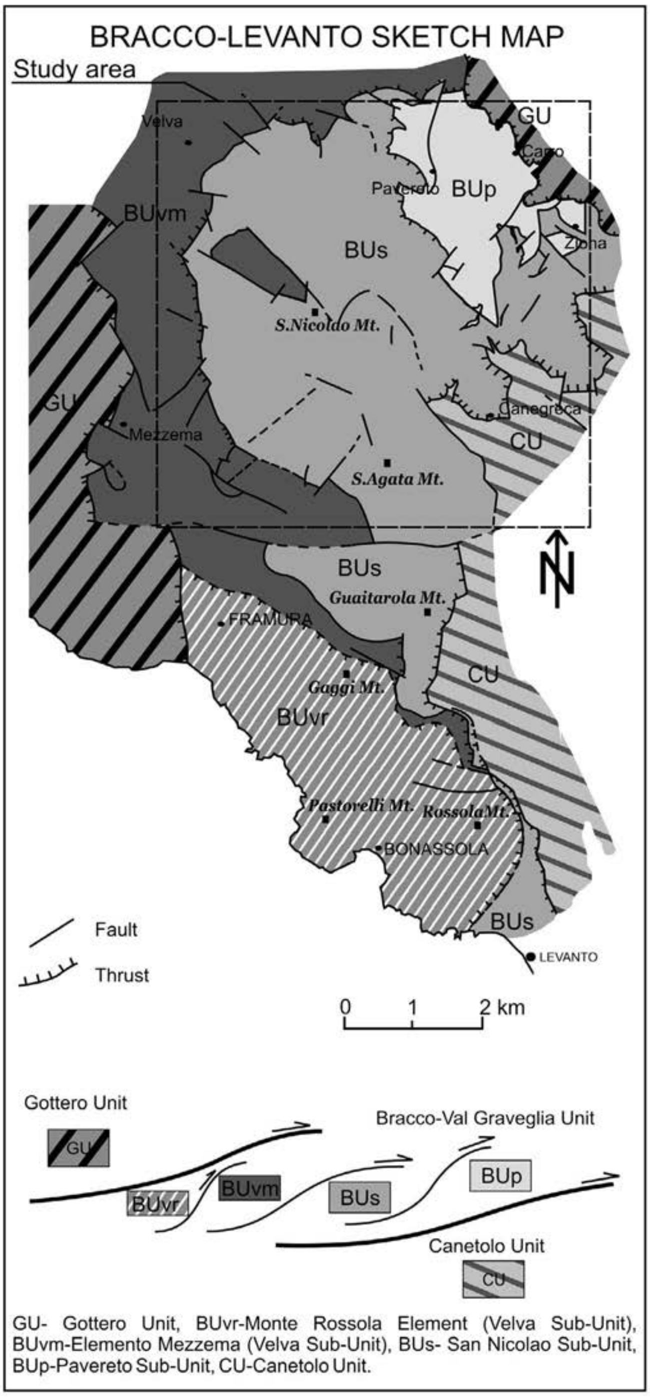

Fig. 2 - Tectonic schematic map of the study area.

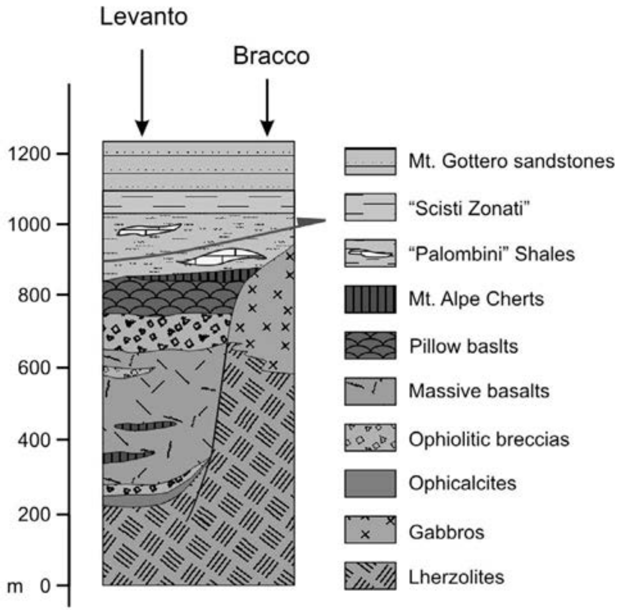

Fig. 3 - Schematic stratigraphic column of the Bracco ophiolitic succession (modified after Principi et al., 2004).

Fig. 4 - "Tectonitic" foliation in the lherzolitic peridotites.

entiates (Cortesogno et al., 1987), represented by plagioclase peridotites and dunites. The gabbros s.l. are the more frequent lithotypes inside the BGC (Fig. 5). Macroscopic features are various and may change rapidly within a few meters. Leucocratic terms prevail, mesocratic ones are more rarely found. Pyroxene gabbros are more diffused than olivine/troctolitic gabbros: both types generally occur next to the plagioclase peridotites. Crystal dimensions may vary from one millimeter, in the microgabbros, up to some centimeters (maximum 15 cm), in the pegmatoid terms, nearly always represented by pyroxene gabbros. In the troctolites, crystals have generally small sizes (5-10 mm).

From a petrographic point of view, pyroxene gabbros ("eufotide" gabbros: Cortesogno et al., 1987, and references therein) are the most widespread if compared with olivine gabbros and troctolites. They are composed by plagioclase (60-75% of total rock), with a rare andesine-labradoritic composition, more frequently characterized by anorthite content of An_{60} (Cortesogno et al., 1987). Pyroxenes (20-

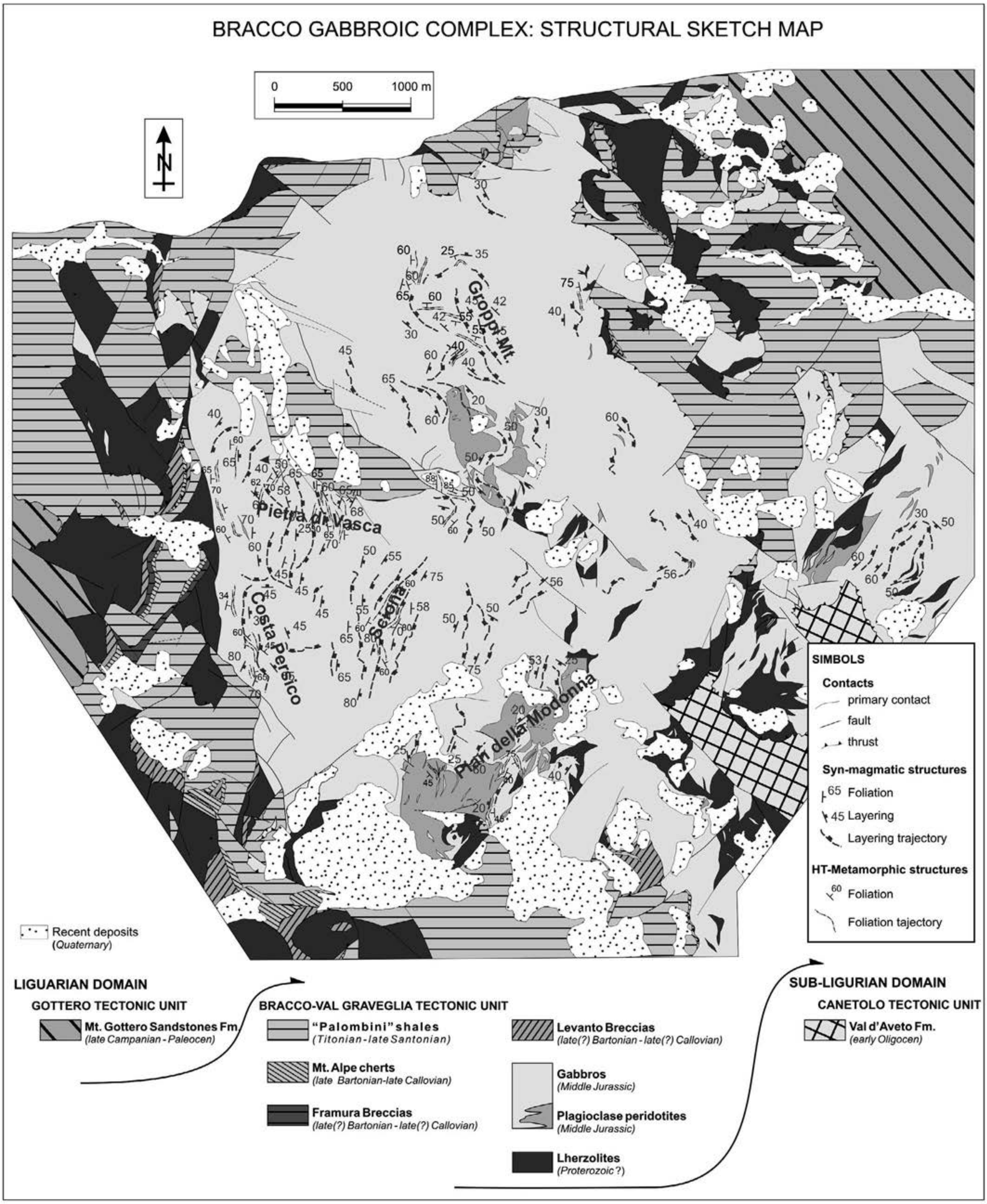

Fig. 5 - Structural sketch map of the Bracco area.

30%) are mainly represented by clinopyroxenes (diopside), inside which the orthopyroxenes may be present as intergrowths, transformed into chlorite. Rarely associated to these textures, small inclusions of red-brown amphiboles (Ti-pargasite) have been observed. Olivine, if present (< 5-10%), is almost completely serpentinized. Ilmenite, Ti-oxide, chrome spinel and rare apatite also occur. The pyroxene gabbros are generally characterized by a macro-granular ipidiomorphic texture, with idiomorphic plagioclase and interstitial to poikilitic clinopyroxene (Fig. 6). Olivine, if pre-

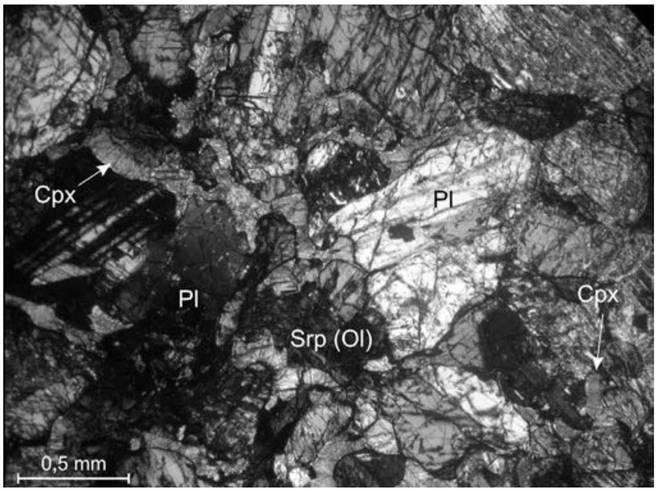

Fig. 6 - Photomicrograph (nicols +) of a typical pyroxene gabbros texture.

sent, is allotriomorphic to sub-idiomorphic. The olivine gabbros are constituted by a generally idiomorphic An_{60-65} plagioclase (more than 60%), olivine (25%), which is more or less "lobate" (Cortesogno et al., 1987) and interstitial or poikilitic, if present, clinopyroxenes (10-15%). In the troctolites the plagioclase, generally with An_{65}, from idiomorphic to sub-idiomorphic, is minor than 40%, idiomorphic olivine is more than 50%, while clinopyroxene (endiopside-diopside) represents 5% or less. In the olivine gabbros and in the troctolites chrome spinels, Ti-oxides and ilmenite can be recognized as accessories.

Mesoscopically, the gabbros *s.l.* can be isotropic or characterized by planar anisotropies as well. Moreover, textural or compositional either gradual or sharp variations, localized in lenticular pockets inside the isotropic gabbro, may occur. The planar anisotropies are interpreted as a magmatic layering, that can be represented either by compositional or granulometric variations This layering can be followed continuously in the outcrop for several meters and may close lenticularly or, other times, fades to apparently isotropic portions. Inside the magmatic layering, a syn-magmatic foliation, sub-parallel or forming a small angle (5-20°) with the layering, often occurs (Fig. 7). The contacts between layered and isotropic gabbro are generally irregular, often gradual, rarely sharp. The magmatic layering very often marks the transition between the gabbro *s.l.* and the plagioclase peridotites and/or dunites, which corresponds to a progressive decrease of plagioclase and to an increase of the femic minerals determining a massive rock dark blue-black in colour at the fresh cut, with a grey-light brown alteration coating, forming lenticular masses inside the gabbros. The composition may range from melatroctolites to dunites (or wehrlites), with idiomorphic to subidiomorphic, locally isoriented olivine (65-95%), poikilitic to sub-idiomorphic plagioclase (5-30%), generally diopsidic Mg-rich clinopyroxene (0-10%), often forming rims between olivine and plagioclase, and chromite (Cortesogno et al., 1987). The chromite, if present, can form isolated generally sub-idiomorphic grains (0.2-4 mm), sometimes showing reabsorption textures into the plagioclases, the clinopyroxenes and the olivines. Other times chromite represents an intercumulus phase among the olivine grains (Bezzi and Piccardo, 1971; Cortesogno et al., 1987). Chromite can be typical in these lithotypes and may also become the prevailing phase, forming continuous metric levels (e.g., Pian della Madonna), with a concentration of euhedral to subhedral crystals in an olivine+plagioclase matrix.

In the BGC, the magmatic layering is often crosscut by gabbroic or dioritic generally fine-grained dykes, from 10 to 70 centimetres thick; some high temperature metamorphic mylonitic shear zones, from some centimetres up to some tens of meters thick, crosscut the BGC as well. The shear zones, in turn, are locally crosscut, together with the hosting gabbro, by basalt dikes, characterized by a non-uniform distribution and density, while they have never been observed inside the lherzolitic peridotites nor in the plagioclase peridotite. The dykes prevalently crop out in two areas: between Costa Persico and Monte San Nicolao and between Monte Groppi (Fig. 8) and Passo della Mola. Their thickness is comprised between some centimetres and 3-4 m and their extension may vary from some decimetres to some hundreds of meters; they can be isolated or arranged in sets. The basalt dykes are massive grey-green to brown rocks, characterized by a porphyric, sometimes aphyric texture, with plagioclase (up to 2-3 cm) and, more rarely, olivine phenocrysts (0.2-0.5 mm; Cortesogno and Gaggero, 1992). The primary contacts with the hosting gabbros are generally marked by sharp linear surfaces, characterized in the basalts, by the typical "chilled margin" textures. The intrusion of the basalts follows the development of the mylonitic high-temperature shear zones.

Very often, next to the basalt dykes, some veins filled by an association of hornblende and oligoclase (Cortesogno et al., 1987), can be observed (Fig. 9); their formation is contemporaneous with that of the dykes, as they are observed to cross the dykes and vice versa. The hornblende-oligoclase

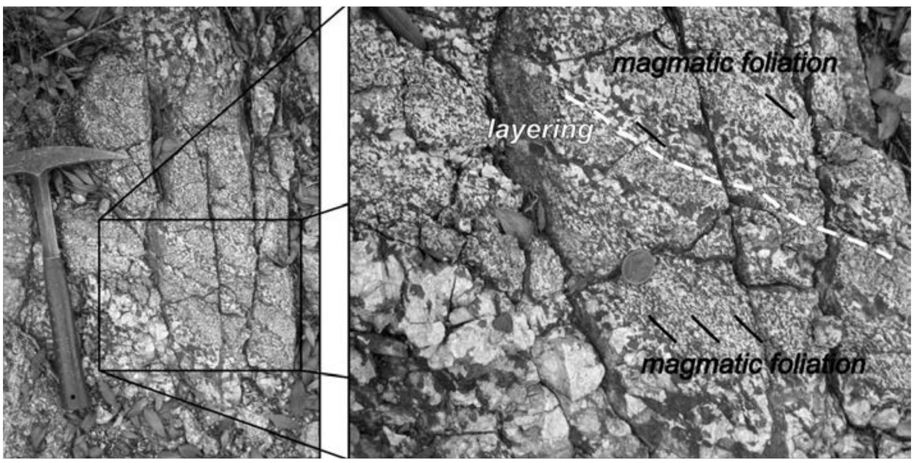

Fig. 7 - Interference between magmatic foliation and layering surfaces.

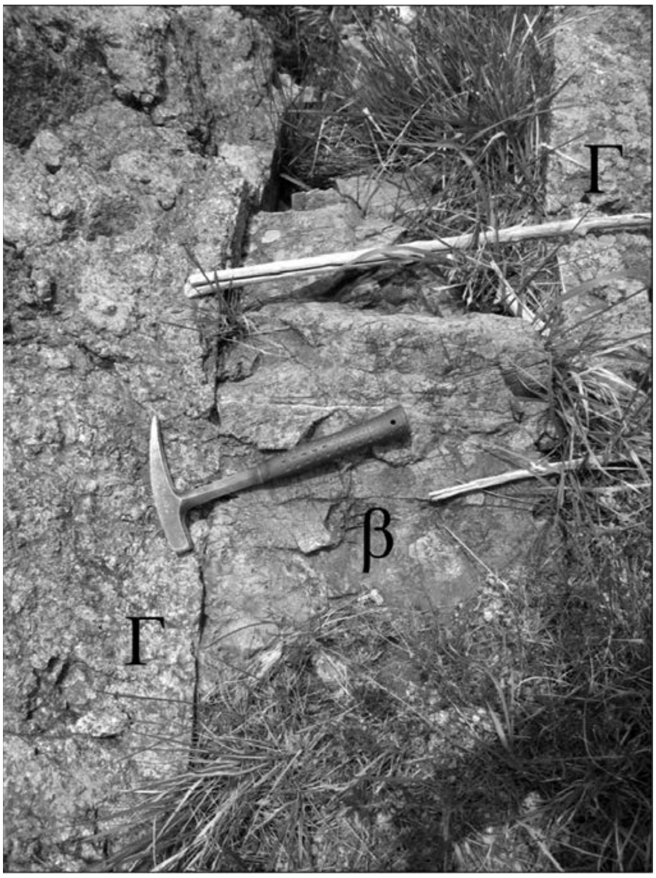

Fig. 8 - Basalt dyke crosscutting the gabbro near Mt. Groppi.

veins can also be developed along the gabbro/basalt contact.

The maximum thickness of the BGC can be evaluated in about 800-1000 m. No primary contacts between the gabbroic complex and the Jurassic sedimentary covers have been observed at the map scale, even if a direct transition from the BGC to some intensely fractured and hematitized gabbros, more rarely to actual gabbro breccias, can locally occur (e.g., Monte Pietra di Vasca).

STRUCTURAL HISTORY

The structural evolution of the BGC is very complex and characterised by the superimposition of several deformative events, developed in different geodynamics contests and related to a retrograde exhumations path.

Magmatic stage

Syn-magmatic deformations, in theory, should show neither deformation nor, above all, recrystallizations in the individual crystals (Nicolas, 1987; 1989; Paterson et al., 1989). Instead, the deformative episodes, developed under metamorphic conditions, are always testified by intra-crystalline deformations ("*plastic strain in crystals*": Nicolas, 1992), represented by dislocation, mechanical twinning and total or partial recrystallization.

The field observations in the BGC, supported by petrographic analyses, led to outline a deformative evolution that started in the early magmatic phases. In fact, besides the magmatic layering, also foliations, lineations, S-C shear zones and folds developed in pre-metamorphic deformative conditions, can be copiously recognized, both in the gabbros and in its femic differentiates.

The magmatic foliation is not homogeneously distributed in the studied area, but it is confined to distinct volumes of rock, generally characterized also by a more or less developed magmatic layering (Fig. 7). At the mesoscale, this foliation consists of millimetric-centimetric levels of variable thickness richer in plagioclase, alternating with levels richer in pyroxenes. Both minerals generally result elongated along the main foliation direction. Plagioclase crystals sometimes form "ribbon"-like discrete monomineralic layers, up to 20-30 cm long. In the dunitic and troctolitic intercalations, due to their chromatic homogeneity, the magmatic foliation is difficult to recognize at the mesoscale and only when a significant amount of plagioclase is present. Layering and magmatic foliation generally form small angles, between 5° and 20°, more rarely, they are parallel. Where the foliation is better developed, incipient transpositive phenomena, involving the layering and/or the contacts between the gabbro and its femic differentiates, can be recognized. On a few well exposed surfaces, where the foliation plane can be observed, magmatic lineations are visible (Fig. 10). They are formed by alignments of minerals, mainly pyroxenes and sometimes plagioclases, arranged along a preferential direction, likely parallel to the magma flow direction. More commonly, instead, structures interpreted as syn-magmatic S-C shear zones (Nicolas, 1992), have been recognized (Fig. 11). They frequently develop at the interface between layering and magmatic foliation, the "C" surface be-

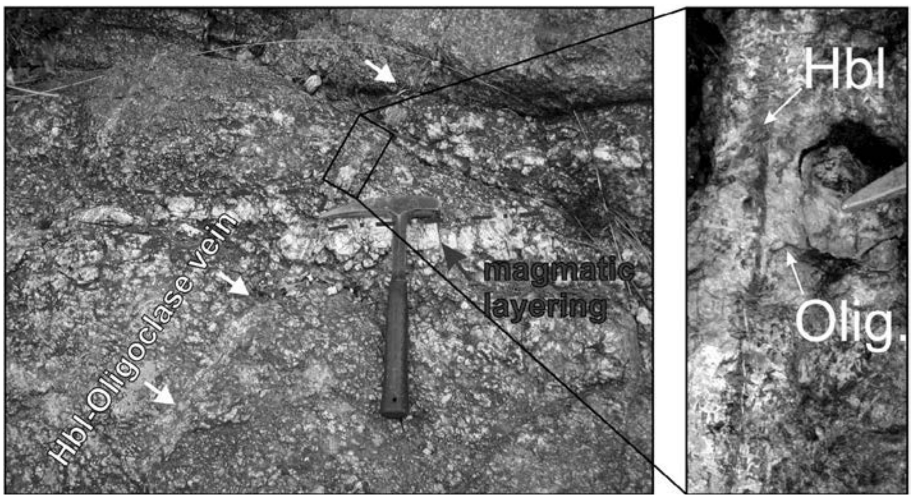

Fig. 9 - Hornblende-oligoclase vein in gabbro.

Fig. 10 - Sample showing magmatic lineations (white lines) marked by plagioclases in the gabbro.

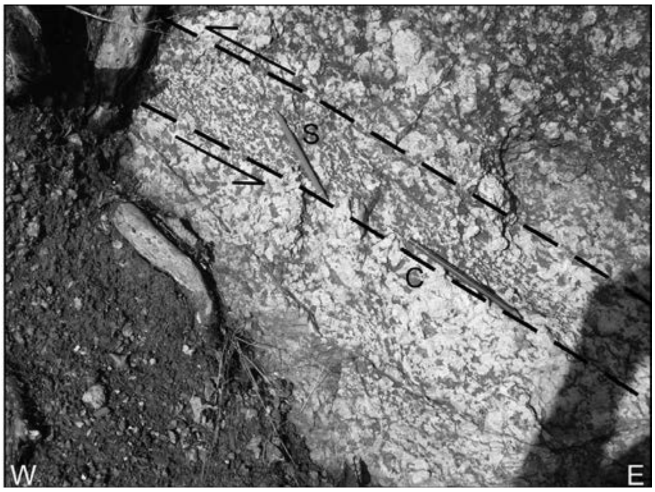

Fig. 11 - Syn-magmatic S-C shear zone near Pietra di Vasca.

ing represented by the layering and the "S" surface by the foliation. In all the outcrops characterized by these structures, an outcrop-scale systematic congruence in the direction of tectonic transport can be observed. The observed syn-magmatic folds may involve both the layering and the foliation, being respectively gentle in the first case and very tight, up to isoclinal, in the second one. The axes of the intrafoliar folds, for a certain volume of rock, generally show little dispersion.

From the petrographic point of view, the more interesting observations come from the gabbroic lithotypes. The magmatic foliation consists of alignments of plagioclase and olivine along preferential directions. Despite the generalized serpentinization of olivine, its primary habitus can be locally recognized, particularly where the mineral is surrounded by undeformed poikilitic pyroxene. Very often the foliation can also be made by alignment of pyroxenes, showing a pronounced isorientation, without evident metamorphic recrystallization.

In many of the studied magmatic foliations, plagioclase crystals are not simply elongated and oriented parallel to a preferential direction, but often, particularly the bigger ones, show internal deformations (mechanical twinning and kink-bands) and/or jointing, sometimes sealed by plagioclase and/or interstitial pyroxenes (Cortesogno et al., 1987). Still, the big deformed crystals (plagioclase and pyroxenes) show compositions analogous to those of the smaller deformed ones.

Clinopyroxenes may be flattened along the foliation, sometimes also elongated parallel to a preferential direction, which has been interpreted as a magmatic lineation. In these cases, as observed by Cortesogno et al. (1987), the clinopyroxenes show internal deformations and an "undeformed peripheral zoning, interstitial with respect to plagioclase and olivine".

Oceanic metamorphic stage

A very complex metamorphic evolution followed the intrusion and the syn-magmatic deformation of the gabbroic complex. Based on mainly petrographic and microstructural observations, three metamorphic phases were distinguished, the first one associated to ductile shear deformations, the other two related prevalently to static recrystallizations, only rarely dynamic. Most of the observations and samples derive from the gabbroic lithotypes, in which the deformations associated to the first two events are more easily detectable.

M_1\D_1 Phase

The oldest metamorphic event M_1 is testified by ductile shear zones (Cortesogno et al., 1987; 1994; Hoogerduijn-Strating, 1988; Molli, 1992; 1994; 1996), developed after both the layering and the other syn-magmatic structures.

The D_1 shear zones, widespread inside the BGC, can be observed also inside its femic differentiates and are concentrated along discrete surfaces, which rarely isolate undeformed volumes of rock and may be at times found along the contacts between the gabbros and the femic rocks (Fig. 12).

Inside the gabbro, the D_1 shear zones, are mainly characterized by the development of a very clear S_1 tectonic pervasive foliation, at the sub-millimetric/millimetric scale, marked by the alternance of white (plagioclase) and dark (pyroxenes) levels. The shear zones generally show a progressive increase of the deformation from the external sectors towards the internal ones (Fig. 13) and are responsible for the gradual deflection of foliation (Ramsay and Graham, 1970; Simpson and Schmidt, 1983). The geometric relations between the shear zones and the associated oblique foliations resulted to be excellent shear sense indicators. Associated to these geometries, S-C structures (Berthé et al., 1979a; 1979b; Vernon et al., 1983; Lister and Snoke, 1984; Krohe, 1990; Passchier and Trouw, 1996) were frequently observed. L_1 "stretching lineations" (Passchier and Trouw, 1996), are often very evident on the S_1 foliation plane, prevalently marked by elongated clinopyroxene porphyroclasts and by more or less continuous ribbons of plagioclase.

Associated to the shear zones, intrafoliar folds, considered synchronous with the D_1 event and generally coupled to the more evolved metamorphic fabrics (Fabric II e III, see below), are sometimes recognizable. Thickness of the shear zones may vary from a minimum of 5-10 cm up to several meters, with length comprised between some decimetres and some tens of meters. In the gabbros, they were frequently observed where the layering is better developed, generally characterized also by magmatic foliations. Attitudes of metamorphic and magmatic foliations result often sub-parallel. The D_1 shear zones have been rarely observed to cross pegmatoid gabbros, characterized by multicentimetric crystals; more commonly they deflect around these domains, which are nearly undeformed. When metamorphic and mag-

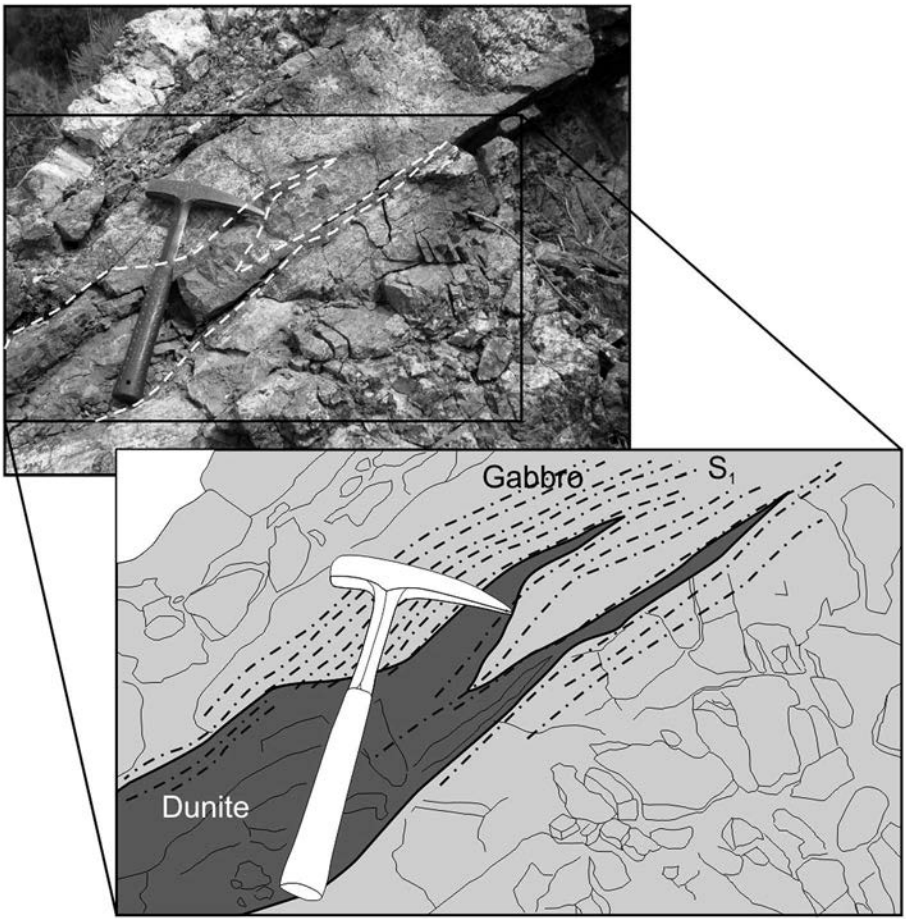

Fig. 12 - Shear zone and transposition-related fabric developed along the contact between dunite and gabbro.

Fig. 13 - Mylonitic D_1 shear zone in the gabbros.

matic foliations are parallel, it is not possible to discriminate between the two fabrics in the field and the observed anisotropy essentially corresponds to a composite foliation.

The gabbroic lithotypes, when crossed by the shear zones, undergo a remarkable internal mineralogic and microstructural reorganization, which determines the development of a mylonitic fabric (Bell and Etheridge, 1973; Hobs et al., 1976; White et al., 1980; Tullis et al., 1982; Hanmer and Passchier, 1991; Passchier and Trouw, 1996). A dimensional decrease of the grain size, together with a progressive development of a more defined foliation, formed by an alternance of plagioclase and pyroxene levels, takes place. Textural and paragenetic magmatic relics, in variable amounts, are often preserved from metamorphic recrystallization. Primary plagioclase undergoes recrystallization, forming polygonal aggregates with 120° triple junctions and a progressive decrease of CaO content (plagioclase recrystallized during the first deformation phase shows an anorthite content comprised between An_{68} and An_{42}; Table 1). Magmatic clinopyroxenes, prevalently diopside (Fig. 14; Table 2), recrystallize into aggregates of secondary pyroxene, with diopsidic composition (Fig. 15; Table 2) and triple junctions with 120° angles. Compared to the primary magmatic pyroxenes, the newly formed ones show an evident decrease of Al_2O_3 content. In particular, the neoblastic syn-D_1 pyroxenes display a clear compositional zoning between the rim and the core of the crystals: Al_2O_3 and TiO_2 decrease towards the external portions of the crystal, while CaO tends to increase (Fig. 16 and 17). Crystals of ilmenite and red-brown amphiboles (Ti-pargasite) may be locally associated to the clinopyroxene neoblasts (Fig. 18) and show triple junctions with secondary

Table 1 - Selected electron microprobe analyses

sample	SC3/8	SC3/8	SC3/8	SC3/8	SC3/8	MOL12	MOL12	MOL12	PV8\9	PV8\9	PV8\9	PER8BB	PER8BB	PV8\9	PV8\9	PV8\9	PV8\9	CAN6A	CAN6A	CAN6A	CAN6A
spot	1D	1E	3B	3BB	4B	3A	4A	4B	2C	2D	3D	6A	6C	7L	9A	9B	7M	4A	4B	4C	4D
phase	D_1	D_1	D_1	D_1	D_1	D_1	D_1	D_3	D_1	D_1	D_1	magm.	magm.	D_1	D_1	D_2	D_1	D_2	D_2	D_2	D_2
oxides (%)																					
SiO_2	53.84	52.81	53.99	51.49	53.11	55.67	53.84	64.09	55.79	55.34	55.53	53.32	51.82	58.87	54.68	61.64	55.76	55.65	55.40	55.71	55.79
Al_2O_3	30.24	30.48	30.26	31.58	30.67	28.83	29.75	23.44	29.13	28.87	29.18	30.62	30.85	23.35	29.55	25.29	29.35	29.21	29.15	29.42	29.03
FeO	0.08	0.23	0.09	0.23	0.19	0.07	0.22	0.00	0.07	0.18	0.14	0.08	0.13	0.73	0.31	0.31	0.28	0.04	0.03	0.05	0.09
TiO_2	0.00	0.06	0.01	0.08	0.08	0.04	0.10	0.00	0.04	0.06	0.03	0.06	0.00	0.07	0.00	0.00	0.04	0.03	0.04	0.03	0.01
Cr_2O_3	0.03	0.01	0.01	0.00	0.00	0.05	0.00	0.06	0.00	0.00	0.09	0.00	0.00	0.03	0.03	0.00	0.00	0.00	0.00	0.00	0.00
MnO	0.00	0.01	0.00	0.00	0.00	0.05	0.00	0.00	0.01	0.02	0.02	0.00	0.00	0.00	0.00	0.00	0.00	0.04	0.02	0.00	0.05
MgO	0.00	0.07	0.01	0.01	0.04	0.01	0.01	0.01	0.00	0.00	0.03	0.02	0.05	2.15	0.03	0.04	0.03	0.01	0.01	0.01	0.00
CaO	12.72	13.23	12.84	14.10	13.15	10.93	12.40	4.66	11.06	11.19	11.50	12.79	13.94	9.96	11.87	6.55	11.12	11.53	11.28	11.47	11.47
Na_2O	4.63	4.20	4.50	3.62	4.25	5.52	4.72	8.86	5.24	5.27	5.31	4.24	3.64	6.68	5.01	8.20	5.41	5.19	5.18	5.16	5.32
K_2O	0.00	0.03	0.00	0.05	0.01	0.01	0.04	0.00	0.06	0.06	0.01	0.00	0.01	0.05	0.03	0.05	0.05	0.01	0.02	0.00	0.00
Total	101.53	101.11	101.72	101.16	101.50	101.18	101.08	101.12	101.41	100.98	101.83	101.14	100.44	101.90	101.51	102.08	102.03	101.72	101.14	101.86	101.77
cations																					
Si	2.40	2.37	2.40	2.32	2.38	2.48	2.41	2.80	2.48	2.47	2.46	2.39	2.34	2.66	2.44	2.69	2.47	2.47	2.47	2.47	2.47
Al	1.59	1.61	1.59	1.68	1.62	1.51	1.57	1.21	1.52	1.52	1.53	1.62	1.65	1.24	1.55	1.30	1.53	1.53	1.53	1.53	1.52
Fe	0.00	0.01	0.00	0.01	0.01	0.00	0.01	0.00	0.00	0.01	0.01	0.00	0.00	0.03	0.01	0.01	0.01	0.00	0.00	0.00	0.00
T	3.99	4.00	3.99	4.00	4.00	4.00	3.99	4.00	4.01	4.00	4.00	4.01	3.99	3.93	4.00	4.00	4.01	4.00	4.00	4.00	3.99
Ca	0.61	0.64	0.61	0.68	0.63	0.52	0.60	0.22	0.53	0.54	0.55	0.61	0.68	0.48	0.57	0.31	0.53	0.55	0.54	0.54	0.54
Na	0.40	0.37	0.39	0.32	0.37	0.48	0.41	0.75	0.45	0.46	0.46	0.37	0.32	0.59	0.43	0.69	0.46	0.45	0.45	0.44	0.46
K	0.00	0.00	0.00	0.00	0.00	0.00	0.00	0.00	0.00	0.00	0.00	0.00	0.00	0.00	0.00	0.00	0.00	0.00	0.00	0.00	0.00
Y	1.01	1.00	1.00	1.00	1.00	1.00	1.01	0.97	0.98	1.00	1.00	0.98	1.00	1.07	1.00	1.00	0.99	0.99	0.99	0.99	1.00
T+Y	5.00	5.00	5.00	5.00	5.00	5.00	5.00	4.97	4.99	4.99	5.00	4.99	4.99	5.00	5.00	5.00	5.00	4.99	4.99	4.99	5.00
An	60.28	63.41	61.17	68.08	63.05	52.21	59.06	22.52	53.63	53.84	54.43	62.51	67.86	45.06	56.62	30.52	53.04	55.09	54.53	55.13	54.35
Ab	39.72	36.41	38.83	31.66	36.91	47.71	40.69	77.47	46.03	45.84	45.50	37.46	32.10	54.69	43.21	69.20	46.65	44.84	45.35	44.85	45.64
Or	0.00	0.18	0.00	0.26	0.04	0.08	0.25	0.01	0.34	0.32	0.07	0.03	0.04	0.25	0.17	0.28	0.31	0.07	0.12	0.01	0.01

(Wt%) of plagioclases from gabbros (structural formulae based on 8 oxygens; mineral abbreviations after Kretz, 1983).

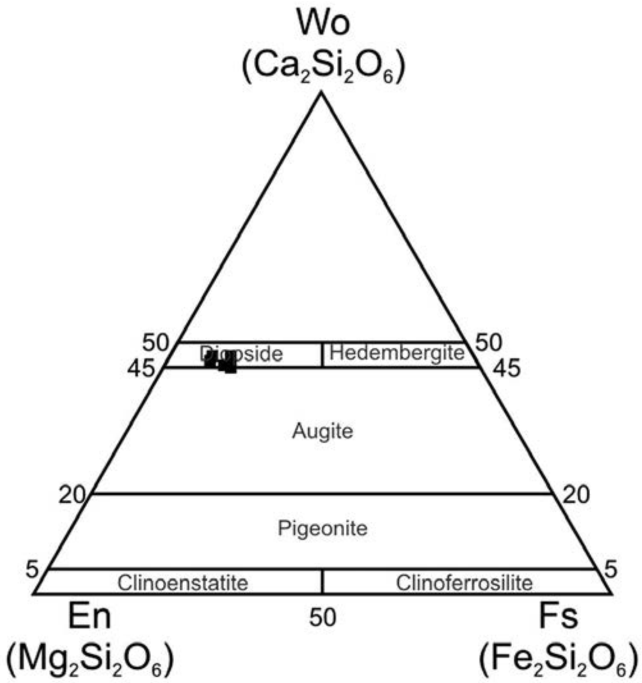

Fig. 14 - Composition of magmatic clinopyroxenes, according to the Morimoto et al. (1988) classification.

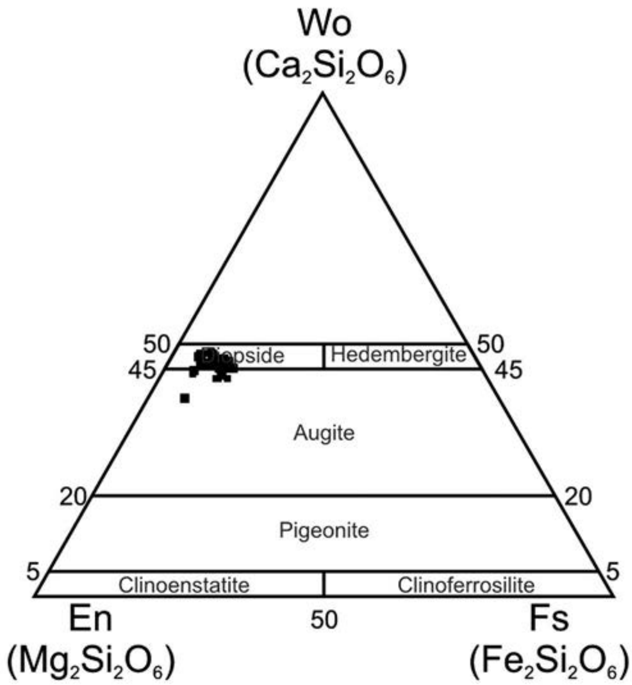

Fig. 15 - Composition of metamorphic syn-D_1 clinopyroxenes according to the Morimoto et al. (1988) classification.

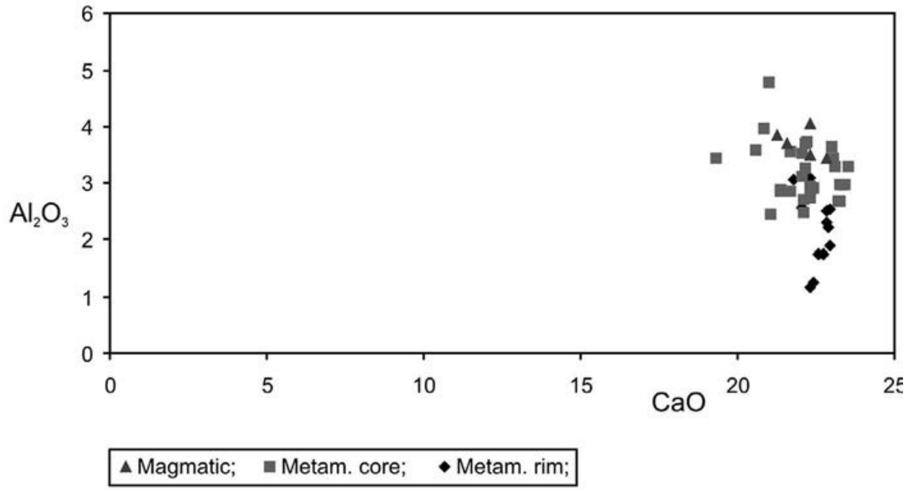

Fig. 16 - Al-Ca diagram for magmatic and syn-D_1 metamorphic clinopyroxenes. For metamorphic ones, the rim/core compositional variation is also plotted.

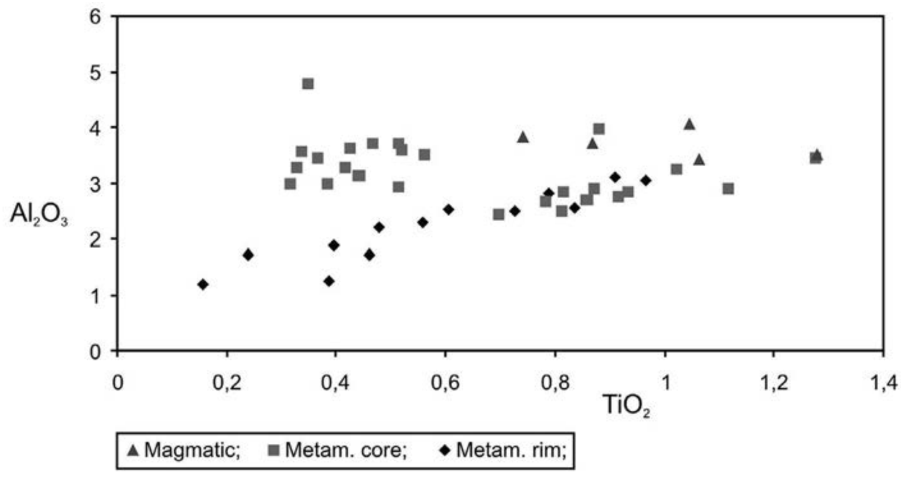

Fig. 17 - Al-Ti diagram for magmatic and syn-D_1 metamorphic clinopyroxenes. For metamorphic ones, the rim/core compositional variation is also plotted.

Table 2 - Selected electron microprobe analyses

sample	SC3/8	SC3/8	SC3/8	MOL12	MOL12	MOL12	MOL12	SNIC1	SNIC1	SNIC1	SNIC1	SNIC1	S1	S1	S1	S1	PV89	PV89	PV89	PV89
spot	1A	1AA	2A	2E	2C	2CC	3F	2A	3B	3A	6A	6AA	2D	2A	3B	3C	5B	5C	7C	7D
rim/core	core	rim	core	rim	core	rim	core	core	core	core	core	rim	rim	core	core	core	rim	core	core	rim
phase	magm.	D_1	D_1	magm.	D_1	D_1	D_1	D_1	D_1	D_1	D_1	D_1	magm.	D_1	D_1	D_1	D_1	D_1	D_1	D_1
oxides (%)																				
SiO_2	53.36	52.99	52.18	51.84	52.28	52.04	52.34	54.22	51.51	51.98	52.64	54.10	53.08	52.78	52.91	53.64	53.78	53.20	52.80	52.97
Al_2O_3	2.67	3.10	3.44	3.71	3.26	2.80	2.85	1.19	3.73	3.72	2.93	1.73	3.29	3.57	3.64	2.98	1.88	2.43	2.71	2.55
FeO	3.73	4.32	4.26	6.13	6.10	6.50	6.67	4.44	4.44	4.21	5.25	4.32	3.88	3.49	3.20	2.91	5.36	6.10	6.09	5.65
TiO_2	0.78	0.91	1.28	0.87	1.02	0.79	0.82	0.16	0.47	0.51	0.51	0.24	0.33	0.34	0.43	0.32	0.40	0.70	0.86	0.84
Cr_2O_3	0.52	0.56	0.65	0.86	0.38	0.50	0.42	0.38	0.98	0.90	1.03	0.72	0.77	0.84	0.79	0.96	0.10	0.17	0.04	0.12
MnO	0.18	0.13	0.18	0.14	0.23	0.14	0.28	0.20	0.17	0.12	0.19	0.05	0.13	0.11	0.19	0.13	0.24	0.21	0.19	0.14
MgO	15.81	16.15	15.50	14.87	14.73	15.24	15.18	16.67	15.69	16.06	15.93	16.50	15.65	16.39	16.59	16.30	15.76	16.33	16.04	15.83
CaO	23.26	22.36	23.10	21.58	22.20	22.32	21.70	22.36	22.25	22.20	22.34	22.63	23.53	21.69	23.04	23.40	22.99	21.09	22.15	22.07
Na_2O	0.48	0.53	0.42	0.51	0.58	0.54	0.56	0.52	0.53	0.45	0.55	0.52	0.33	0.33	0.42	0.63	0.39	0.45	0.50	0.47
K_2O	0.00	0.01	0.00	0.00	0.00	0.01	0.00	0.00	0.02	0.00	0.00	0.00	0.00	0.01	0.00	0.01	0.02	0.00	0.01	0.03
Total	100.79	101.06	101.01	100.51	100.77	100.87	100.80	100.13	99.78	100.15	101.38	100.82	100.99	99.53	101.20	101.28	100.92	100.67	101.38	100.66
cations																				
Si	1.94	1.92	1.90	1.90	1.91	1.90	1.91	1.98	1.89	1.90	1.90	1.96	1.92	1.93	1.90	1.93	1.96	1.94	1.91	1.93
Al^{IV}	0.06	0.08	0.10	0.10	0.09	0.10	0.09	0.02	0.11	0.10	0.10	0.04	0.08	0.07	0.10	0.07	0.04	0.06	0.09	0.07
Fe^{3+}	0.00	0.00	0.00	0.00	0.00	0.00	0.00	0.00	0.00	0.00	0.00	0.00	0.00	0.00	0.00	0.00	0.00	0.00	0.00	0.00
sum T	2.00	2.00	2.00	2.00	2.00	2.00	2.00	2.00	2.00	2.00	2.00	2.00	2.00	2.00	2.00	2.00	2.00	2.00	2.00	2.00
Al^{VI}	0.05	0.05	0.04	0.06	0.05	0.02	0.04	0.03	0.05	0.06	0.03	0.03	0.06	0.09	0.06	0.05	0.04	0.04	0.03	0.04
Fe^{3+}	0.00	0.00	0.00	0.00	0.00	0.00	0.00	0.00	0.00	0.00	0.00	0.00	0.00	0.00	0.00	0.00	0.00	0.00	0.00	0.00
Ti	0.02	0.02	0.03	0.02	0.03	0.02	0.02	0.00	0.01	0.01	0.01	0.01	0.01	0.01	0.01	0.01	0.01	0.02	0.02	0.02
Mg	0.86	0.87	0.84	0.81	0.80	0.83	0.83	0.91	0.86	0.87	0.86	0.89	0.85	0.88	0.89	0.87	0.86	0.89	0.87	0.86
Cr	0.01	0.02	0.02	0.02	0.01	0.01	0.01	0.01	0.03	0.03	0.03	0.02	0.02	0.02	0.02	0.03	0.00	0.00	0.00	0.00
Fe^{2+}	0.06	0.04	0.06	0.08	0.10	0.11	0.10	0.05	0.05	0.03	0.07	0.05	0.06	0.00	0.02	0.04	0.09	0.05	0.08	0.07
sum M1	1.00	1.00	1.00	1.00	1.00	1.00	1.00	1.00	1.00	1.00	1.00	1.00	1.00	1.00	1.00	1.00	1.00	1.00	1.00	1.00
Na	0.03	0.04	0.03	0.04	0.04	0.04	0.04	0.04	0.04	0.03	0.04	0.04	0.02	0.02	0.03	0.04	0.03	0.03	0.04	0.03
Mn	0.01	0.00	0.01	0.00	0.01	0.00	0.01	0.01	0.01	0.00	0.01	0.00	0.00	0.00	0.01	0.00	0.01	0.01	0.01	0.00
Ca	0.90	0.87	0.90	0.85	0.87	0.87	0.85	0.87	0.87	0.87	0.87	0.88	0.91	0.85	0.89	0.90	0.90	0.82	0.86	0.86
Fe^{2+}	0.06	0.09	0.07	0.11	0.08	0.08	0.10	0.08	0.08	0.10	0.09	0.08	0.06	0.11	0.08	0.05	0.07	0.14	0.10	0.10
Mg	0.00	0.00	0.00	0.00	0.00	0.00	0.00	0.00	0.00	0.00	0.00	0.00	0.00	0.02	0.00	0.00	0.00	0.00	0.00	0.00
sum M2	1.00	1.00	1.00	1.00	1.00	1.00	1.00	1.00	1.00	1.00	1.00	1.00	1.00	1.00	1.00	1.00	1.00	1.00	1.00	1.00
M1+M2	2.00	2.00	2.00	2.00	2.00	2.00	2.00	2.00	2.00	2.00	2.00	2.00	2.00	2.00	2.00	2.00	2.00	2.00	2.00	2.00
O	6.01	6.00	6.00	6.00	6.00	5.97	5.98	5.99	5.98	5.99	5.98	6.00	6.00	6.02	5.99	5.99	5.99	6.00	5.97	5.99
Q	1.87	1.87	1.87	1.85	1.86	1.90	1.88	1.91	1.87	1.87	1.88	1.90	1.88	1.85	1.87	1.86	1.91	1.90	1.91	1.90
J	0.07	0.07	0.06	0.07	0.08	0.08	0.08	0.07	0.08	0.06	0.08	0.07	0.05	0.05	0.06	0.09	0.06	0.06	0.07	0.07
Wo	48.14	46.28	47.96	45.74	46.59	45.82	44.96	45.45	46.64	46.31	45.80	46.16	48.56	45.85	47.22	48.28	46.62	43.26	44.84	45.38
En	45.55	46.53	44.82	43.87	43.03	43.54	43.79	47.18	45.81	46.63	45.48	46.86	44.97	48.21	47.35	46.81	44.50	46.63	45.21	45.31
Fs	6.31	7.19	7.22	10.39	10.38	10.65	11.25	7.37	7.55	7.07	8.72	6.98	6.47	5.94	5.43	4.91	8.88	10.11	9.95	9.30
NAME	Di	Di	Di	Di	Di	Di	Aug	Di	Di	Di	Di	Di	Di	Di	Di	Di	Di	Di	Di	Di

(Wt%) of pyroxenes from gabbros (structural formulae based on 6 oxygens; mineral abbreviations after Kretz, 1983).

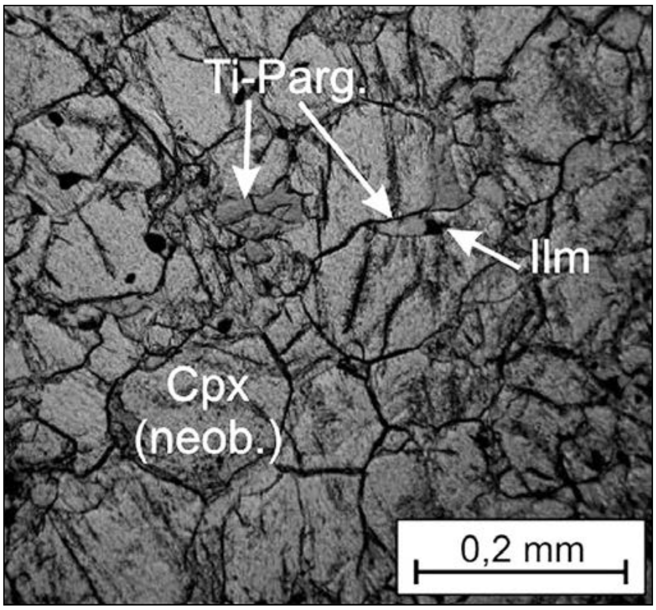

Fig. 18- Interstitial syn-D_1 Ti-pargasite and ilmenite crystals inside a clinopyroxene granoblastic aggregate.

diopside or can be found in the pressure shadows of magmatic diopside. New clinopyroxenes never display cleavage traces nor exsolution lamellae. Anyway, intracrystalline deformations seem to be more frequent in the deformed pyroxenes than in undeformed protoliths.

Drawing on similar petrographic-structural studies (e.g., Molli 1994), based on different meso- and micro-structural features recognized in the analyzed shear zones, four different fabric types were distinguished (Figs. 19 and 20):

Fabric I: the gabbroic protolith is noticeably deformed and shows a very penetrative foliation at the millimetric-centimentric scale, mainly marked by the elongation of clinopyroxene porphyroclasts, locally forming scarcely coalescent lenticular domains. Clinopyroxene porphyroclasts display internal undulations and may be surrounded by a millimetric/sub-millimetric rim of secondary clinopyroxene (0.2 mm), which locally includes elements of the primary mineral. Interstitial little crystals of brown hornblende (Ti-pargasite, Figs. 18, 21 and 22; Table 3) can be recognized inside the clinopyroxene neoblasts. Primary plagioclase frequently shows undulose extinction and mechanical twinning. In general, recrystallization, accompanied by grain size reduction, takes place along the borders of the crystals.

Fabric II: foliation is well developed and pervasive at the millimetric scale, formed by lenticular domains (i.e.: "*flaser* gabbri" or "gabbri occhiadini" of previous authors), of more or less stretched clinopyroxenes, alternated to granoblastic layers of recrystallized plagioclase. Clinopyroxene levels are more or less continuous and characterized by the presence of clinopyroxene porphyroclasts, surrounded by aggregates of new polygonal clinopyroxenes (0.1-0.2 mm), that constitute the pressure shadows. Interstitial brown hornblende is also present. The clinopyroxenes often show internal deformations, such as undulose extinction and micro-

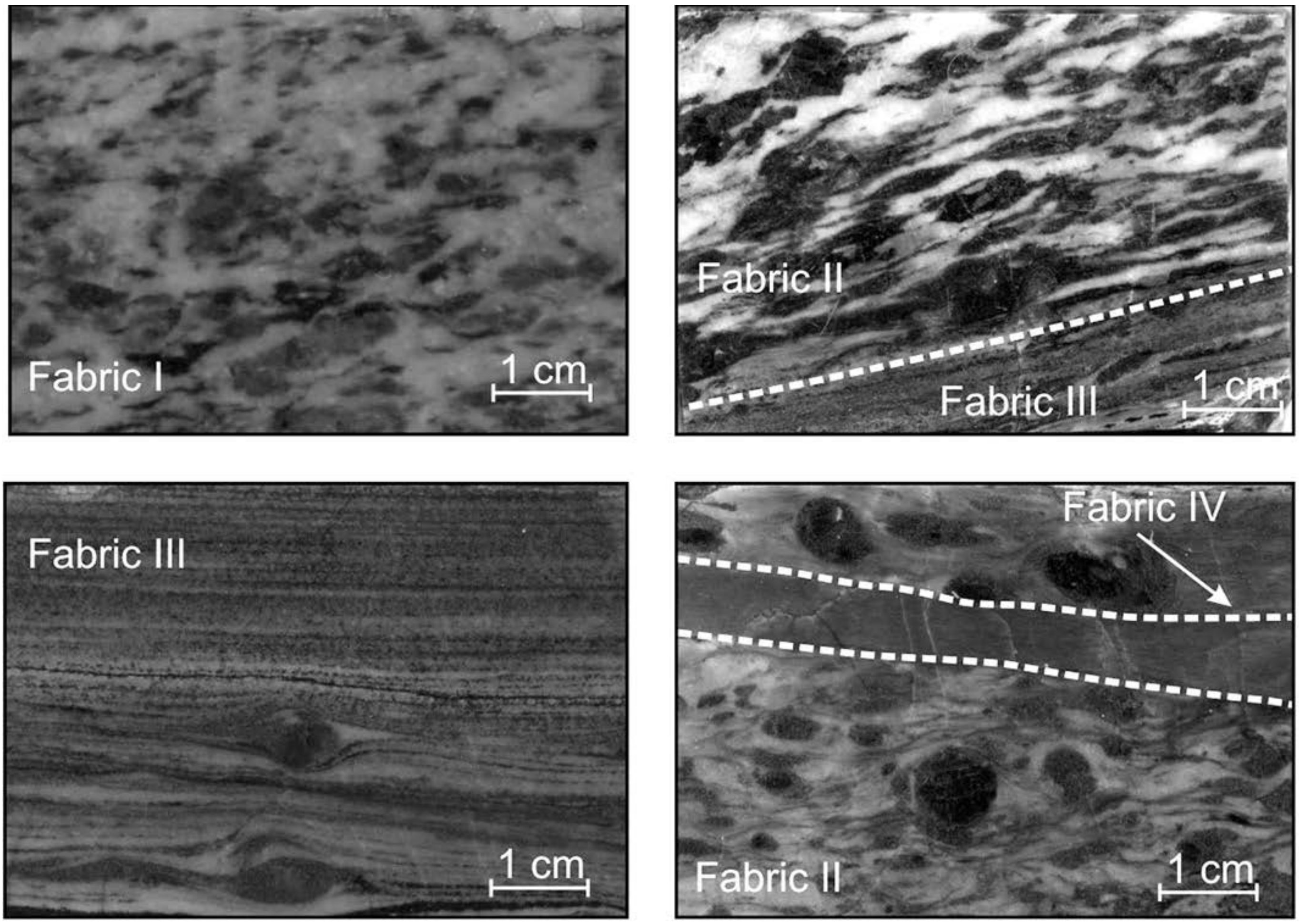

Fig. 19 - Details of textures of *Fabrics I-IV*.

Table 3 - Selected electron microprobe analyses

sample	CAN6A	CAN6A	CAN6A	CAN6A	CAN6A	PV89	PV89	SC3/8	SC3/8	PER8BB	PER8BB	PER8BB	PER8BB	MOL12	MOL12	MOL12	MOL12	MOL12	MOL12	SNIC1	SNIC1
spot	1C	2A	2B	2B	3B	2E	3C	2B	2BB	8A2	5A1	5B	1C	2B	2D	3D	3E	6A	6B	2B	6B
phase	D_2	D_2	D_2	D_2	D_3	D_1	D_1	D_1	D_1	D_3	D_2	D_3	D_3	D_1	D_2	D_1	D_1	D_2	D_3	D_1	D_1
oxides (%)																					
SiO_2	48.24	46.04	47.51	47.20	51.36	42.72	43.12	42.90	43.20	57.61	46.78	53.71	55.13	43.73	48.93	43.38	42.73	51.52	55.27	42.97	42.89
Al_2O_3	9.60	11.91	10.44	11.32	6.50	11.65	11.93	11.99	11.62	1.97	11.71	5.73	3.34	11.58	9.45	11.36	11.61	5.56	2.20	11.53	12.06
FeO	7.55	8.41	7.30	7.71	6.65	8.84	9.02	6.33	6.75	2.10	5.22	4.59	4.00	9.37	10.02	9.65	9.84	9.71	7.45	7.99	7.37
TiO_2	0.89	0.45	0.38	0.52	0.86	4.90	4.16	4.38	3.85	0.03	0.34	0.25	0.72	3.83	0.20	4.13	3.94	0.19	0.17	3.61	3.14
Cr_2O_3	0.00	0.00	0.00	0.00	0.30	0.27	0.11	1.21	1.29	0.04	0.08	0.01	0.39	0.70	0.09	0.70	0.68	0.10	0.03	1.22	1.52
MnO	0.09	0.12	0.10	0.16	0.00	0.12	0.15	0.04	0.10	0.00	0.10	0.09	0.01	0.12	0.13	0.13	0.14	0.17	0.10	0.15	0.13
MgO	17.20	16.36	18.26	16.38	18.42	13.88	14.02	16.01	16.25	23.01	18.21	19.36	20.79	14.40	16.08	14.25	13.95	18.81	20.28	15.43	15.53
CaO	12.71	12.58	11.61	12.75	12.57	11.61	11.87	12.08	11.45	12.21	11.95	13.00	12.47	11.93	11.82	11.49	11.71	10.63	11.59	11.72	11.99
Na_2O	2.03	2.49	1.79	2.20	1.47	3.37	3.00	2.98	2.55	0.33	2.55	0.94	0.75	2.23	1.75	2.89	2.68	0.88	0.32	2.57	2.59
K_2O	0.08	0.12	0.06	0.12	0.05	0.11	0.23	0.05	0.05	0.04	0.05	0.01	0.02	0.14	0.02	0.14	0.09	0.02	0.03	0.06	0.08
Total	98.39	98.48	97.46	98.36	98.19	97.46	97.61	97.97	97.09	97.34	96.97	97.70	97.62	98.01	98.49	98.13	97.37	97.60	97.42	97.26	97.30
cations																					
Si	6.80	6.51	6.61	6.67	7.19	6.23	6.27	6.16	6.19	7.80	6.57	7.46	7.60	6.30	6.86	6.28	6.24	7.08	7.60	6.20	6.19
Al^{IV}	1.20	1.49	1.39	1.33	0.81	1.77	1.73	1.84	1.81	0.20	1.43	0.54	0.40	1.70	1.14	1.72	1.76	0.90	0.36	1.80	1.81
T	8.00	8.00	8.00	8.00	8.00	8.00	8.00	8.00	8.00	8.00	8.00	8.00	8.00	8.00	8.00	8.00	8.00	7.98	7.95	8.00	8.00
Al^{VI}	0.39	0.49	0.32	0.56	0.26	0.23	0.32	0.19	0.15	0.11	0.51	0.40	0.15	0.27	0.42	0.21	0.23	0.00	0.00	0.16	0.24
Ti	0.09	0.05	0.04	0.05	0.09	0.54	0.45	0.47	0.41	0.00	0.04	0.03	0.08	0.41	0.02	0.45	0.43	0.02	0.02	0.39	0.34
Cr	0.00	0.00	0.00	0.00	0.03	0.03	0.01	0.14	0.15	0.00	0.01	0.00	0.04	0.08	0.01	0.08	0.08	0.01	0.00	0.14	0.17
Fe^{3+}	0.21	0.39	0.85	0.17	0.17	0.00	0.00	0.00	0.46	0.24	0.53	0.00	0.17	0.19	0.64	0.13	0.15	1.12	0.86	0.35	0.27
Fe^{2+}	0.68	0.61	0.00	0.74	0.61	1.08	1.10	0.76	0.35	0.00	0.08	0.53	0.29	0.94	0.53	1.03	1.05	0.00	0.00	0.61	0.62
Mn	0.01	0.01	0.01	0.02	0.00	0.01	0.02	0.00	0.01	0.00	0.01	0.01	0.00	0.01	0.02	0.02	0.02	0.02	0.01	0.02	0.02
Mg	3.61	3.45	3.78	3.45	3.84	3.02	3.04	3.43	3.47	4.64	3.82	4.01	4.27	3.09	3.36	3.07	3.04	3.85	4.16	3.32	3.34
C	5.00	5.00	5.00	5.00	5.00	4.91	4.94	5.00	5.00	5.00	5.00	4.98	5.00	5.00	5.00	5.00	5.00	5.02	5.05	5.00	5.00
Ca	1.92	1.91	1.73	1.93	1.88	1.81	1.85	1.86	1.76	1.77	1.80	1.93	1.84	1.84	1.77	1.78	1.83	1.56	1.71	1.81	1.85
Na	0.08	0.09	0.27	0.07	0.12	0.19	0.15	0.14	0.24	0.09	0.20	0.07	0.16	0.16	0.23	0.22	0.17	0.24	0.08	0.19	0.15
B	2.00	2.00	2.00	2.00	2.00	2.00	2.00	2.00	2.00	1.86	2.00	2.00	2.00	2.00	2.00	2.00	2.00	1.80	1.79	2.00	2.00
Na	0.47	0.59	0.21	0.53	0.28	0.77	0.70	0.69	0.46	0.00	0.49	0.19	0.04	0.46	0.25	0.59	0.59	0.00	0.00	0.53	0.58
K	0.01	0.02	0.01	0.02	0.01	0.02	0.04	0.01	0.01	0.01	0.01	0.00	0.00	0.03	0.00	0.02	0.02	0.00	0.00	0.01	0.02
A	0.49	0.61	0.22	0.56	0.29	0.79	0.74	0.70	0.47	0.01	0.50	0.19	0.05	0.49	0.25	0.62	0.61	0.00	0.00	0.54	0.59
Total	15.49	15.61	15.22	15.56	15.29	15.70	15.69	15.70	15.47	14.86	15.50	15.17	15.05	15.49	15.25	15.62	15.61	14.80	14.80	15.54	15.59
NAME	Mg-Hbl	Ed	Mg-Hbl	Ed	Mg-Hbl	Ti-Prg	Ti-Prg	Ti-Prg	Ts	Tr	Ed	Mg-Hbl	Tr-Act	Ts	Mg-Hbl	Ti-Prg	Ti-Prg	Mg-Hbl	Tr	Ti-Prg	Ti-Prg

Mineral analyses were carried out with a Cameca Sx electron microprobe at Laboratorio di Microanalisi, Università di Padova, provided with four wavelength-dispersive spectrometers.
Operating conditions were: 15 kV accelerating voltage and 15 nA sample current.

(Wt%) of amphiboles from gabbros (structural formulae calculated assuming total cation sum minus Ca, Na, K = 13 per anhydrous formula unit; mineral abbreviations after Kretz, 1983).

folds. The pressure shadows developed around clinopyroxene porphyroclasts, sometimes acquire "σ"-geometries (Molli, 1994; Passchier and Trouw, 1996). The plagioclase is highly recrystallized; rare primary crystals display mechanical twinning and undulose extinction. Recrystallization develops prevalently along the borders of the crystals and is associated by a grain size reduction (0.05-0.1 mm).

Fabric III: foliation is well developed and extremely pervasive, formed by a millimetric alternance of clinopyroxene and plagioclase levels, with a significant grain size reduction of clinopyroxenes (0.1 mm) and an extensive dynamic recrystallization of plagioclases (0.05-0.1 mm). Rare magmatic clinopyroxene porphyroclasts are surrounded by abundant clinopyroxene neoblasts, generally forming the pressure shadows, both with "σ" or "δ" asymmetries (Passchier and Simpson, 1986; Passchier and Trouw, 1996) or without asimmetries. Plagioclase crystals are characterized by diffuse recrystallization and acquire a peculiar shape, being concentrated in discrete levels and elongated parallel to a preferential direction, sometimes discordant with respect to foliation. S-C structures, useful to reconstruct the sense of shear, may be locally associated to these fabrics, both inside the plagioclase levels and by the alternances with clinopyroxene levels; in the first case, unconformity is generally highlighted by thin (sub-millimetric) levels rich in oxides (Fig. 20).

Fabric IV: it is very difficult to recognize this foliation at the mesoscale, while it can be identified with the microscopic analysis, which shows a sub-millimetric compositional alternance, between plagioclase and pyroxene levels, with both crystal types generally smaller that 0.05 mm. Sometimes, bigger clinopyroxene porphyroclasts (0.1-0.2 mm), elongated parallel to the main foliation, may occur (Fig. 20). S-C structures, with S surfaces materialized mainly inside the pyroxene levels (Molli, 1994), can be also observed. This fabric corresponds to the "*high strain fabric*" (Molli, 1992) and to the "*flinty ultramylonite*" (Molli, 1994).

The fabrics described above represent the different stages of a deformation gradient and should theoretically correspond to a progressive increase of deformation from the *Fabric I* towards the *Fabric IV*. Yet, in the field, both a gradual and an abrupt transition between the fabrics and even the transition between two non-consecutive terms have often been observed. Sometimes the passage towards more evolved fabric domains is accompanied by the development of intrafoliar folds.

The distribution and attitude of the mentioned structures can intensely vary in the study area, though maintaining a general homogeneous trend for large sectors. Analogously, L_1 stretching lineations show fairly uniform trends in the same areas. D_1 mylonitic gabbros are locally crossed by

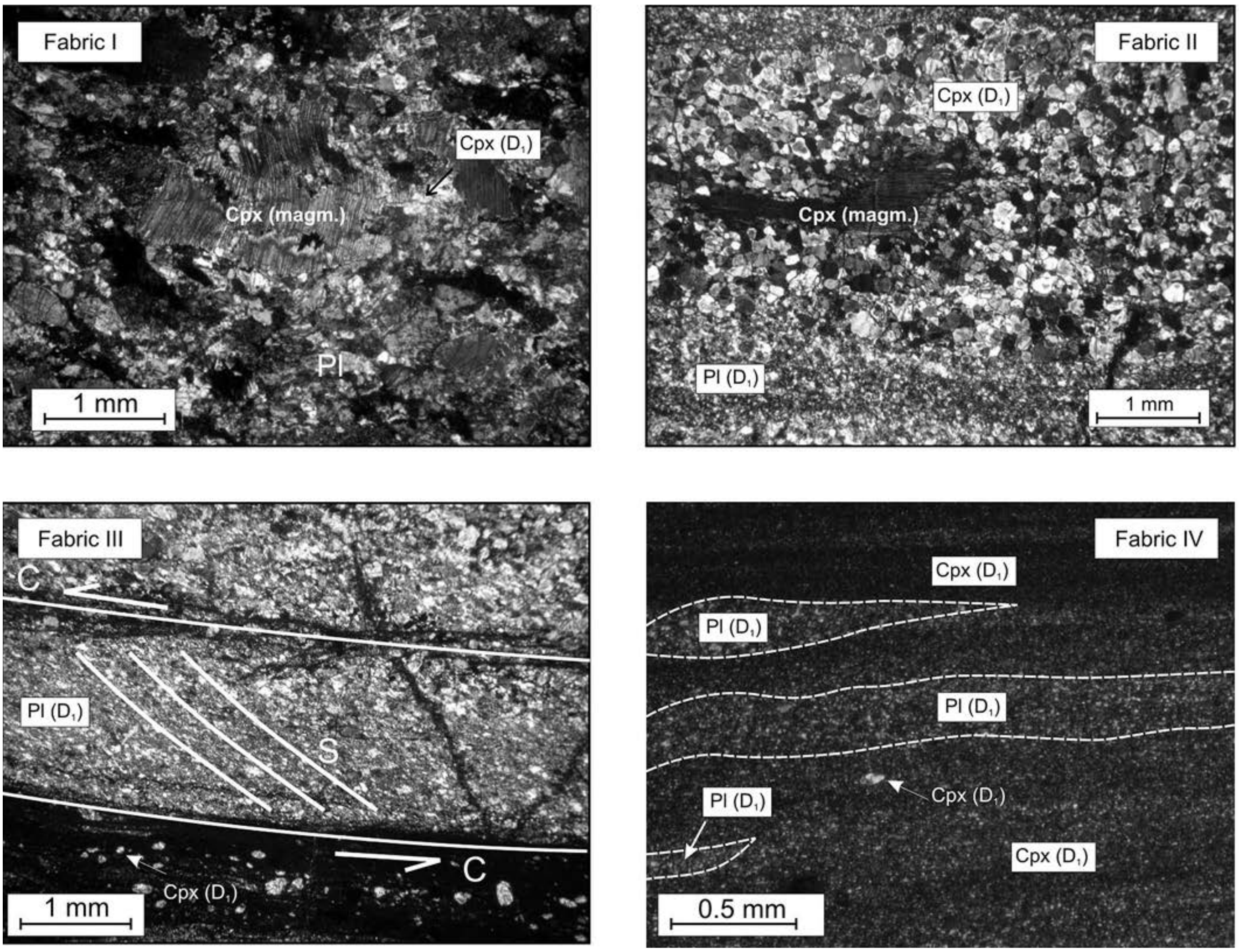

Fig. 20 - Photomicrograph (crossed polars) of typical textures in *Fabrics I-IV*.

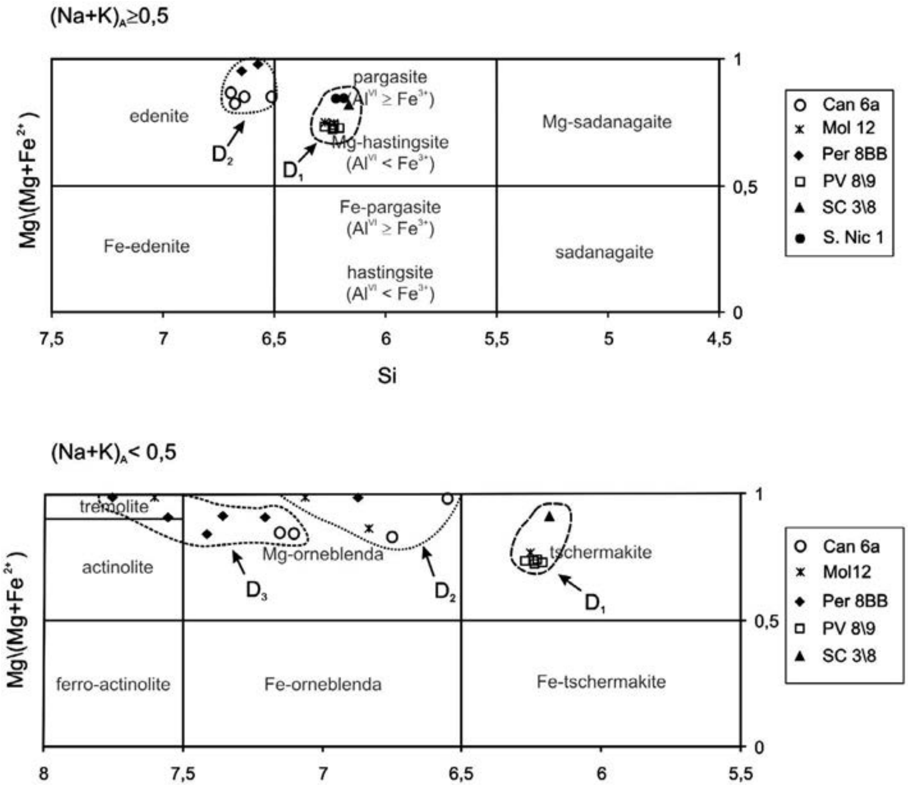

Fig. 21 - Ca-amphiboles composition, according to the Leake et al. (1997) classification.

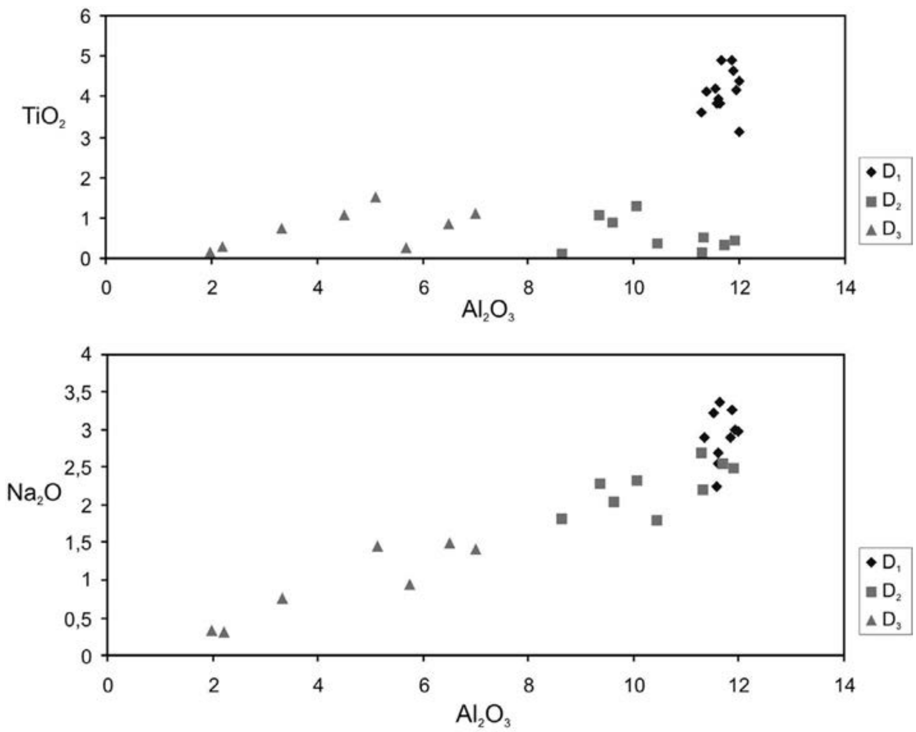

Fig. 22 - Ti vs Al and Na vs Al diagrams for amphiboles belonging to the different metamorphic phases.

veins filled with a hornblende+plagioclase association (Fig. 9), predating their formation. Similarly, also the basalt dykes (Fig. 8) cut the shear zones without suffering deformation, their intrusion being therefore subsequent to the development of D_1 shear zones.

M_2\\D_2 Phase

The second metamorphic phase in the BGC shows variable features. It frequently involves static recrystallizations in the undeformed gabbroic lithotypes and in those affected by D_1 deformations. M_2 metamorphic event is generally testified by the static recrystallization of several metamorphic phases, mainly amphiboles such as Mg-hornblende and edenite (Figs. 21 and 22; Table 3), often pseudomorphic after magmatic pyroxenes.

Yet, this metamorphic event is locally associated to the development of D_2 ductile shear zones (Fig. 23), which are extremely rare with respect to the D_1 ones. Mesoscopically, these structures are formed by sheared gabbros, characterized by a discontinuous foliation, variously penetrative at

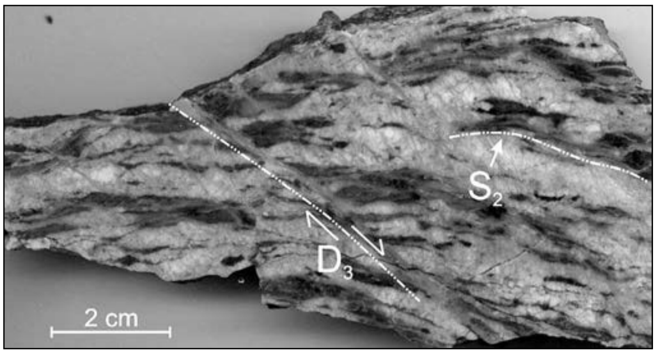

Fig. 23 - Photo of metagabbro sample from a syn-D_2 shear zone.

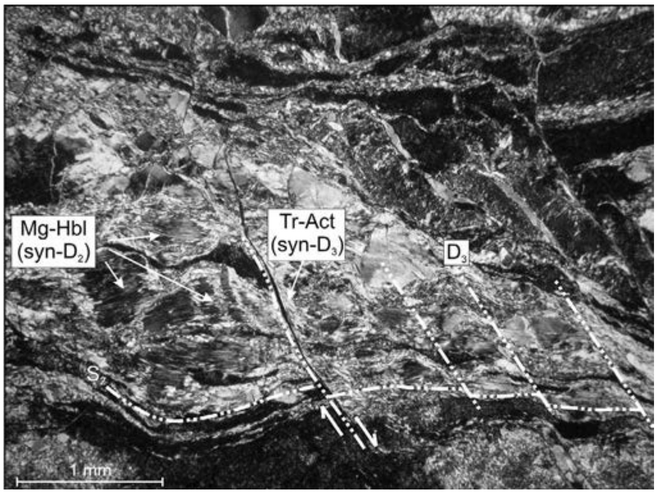

Fig. 24 - Photomicrograph (nicols +) showing interference between syn-D_3 crenulations and S_2 foliation in gabbro. Syn-kinematic tremolite/actinolite develops along the microfault (white dashed line).

the millimetric/centimetric scale and materialized by alternations of white plagioclase levels and green amphibole ones. Thickness is extremely variable (0.5 - 4 m), while extension is very limited, with a maximum of 10-15 m. In the few cases observed in the field, syn-D_2 shear zones develop along previous metamorphic syn-D_1structures. S-C structures and intrafoliar folds have been locally observed. When present, L_2 stretching lineations are marked, on S_2 schistosity, by the elongation of amphiboles. From the microscopic point of view, these shear zones are characterized by a textural and mineralogic reorganization, which causes the development of mylonitic fabrics, consisting of a grain size reduction of both magmatic and metamorphic minerals and of a locally defined foliation, marked by the alternation of lepidoblastic/nematoblastic amphibole levels (± relics of pyroxene) and granoblastic levels of plagioclase. Plagioclases display internal deformations, with mechanical twinning and intense cataclasis, which causes an evident reduction of grain size, yet lower than in D_1 phase. Retrogressive transformation of pyroxenes into amphiboles, mainly Mg-hornblende, starts in static conditions and continues during the D_2 deformation. In fact, deformed and rotated Mg-hornblende, with syn-kinematic recrystallization of similar syn-D_2 amphiboles in the pressure shadows, together with tremolite and chlorite, are almost common. Plagioclase often preserve relatively high contents of Ca (An_{57-58}, Table 1), while the more recrystallized ones show low Ca contents ($An_{<30}$, Table 1). An early development of syn-kinematic hornblende in the pressure shadows of syn-D_1 pyroxenes can rarely occur. Newly formed syn-D_2 amphiboles grow onto the D_1 pyroxene neoblasts, resulting parallelized to the D_1 trend of deformations.

Being the record of syn-D_2 mylonites too scarce, it was not possible to develop a fabric classification as for the M_1 event.

Younger mineralogic phases, developed at the end of the D_2 event, correspond mainly to acicular amphiboles (tremolite-actinolite), statically or dynamically recrystallized in the more external portions of the pressure shadows and often associated to chlorite.

The D_2 are locally crossed by veins filled with Mg-hornblende and/or associations with green amphiboles (tremolite-actinolite) ± plagioclase, epidote and prehnite-pumpellyite. Veins filled with serpentine and/or chlorite were observed both crosscutting the $M_2\backslash D_2$ mineral assemblages or structures and, in other cases, being displaced and boudinated by the D_2 deformations. Given the scarcity of D_2 structures in the study area, the intersection between them and the basalt dykes has never been observed. Yet, veins filled with hornblend + oligoclase, deformed by the D_2 phase (with syn-kinematic blastesis of green to colourless hornblende in pressure tails of primary brown to colourless hornblende) have been locally observed.

$M_3\backslash D_3$ Phase

This event is commonly represented by static recrystallizations, very rarely dynamic, of new minerals, prevalently amphiboles. In particular, the growth of green to colourless amphiboles (tremolite-actinolite, Figs. 21 and 22, Table 3) onto primary femic or metamorphic syn-$D_1\backslash D_2$ minerals, until their quite complete substitution, has been attributed to this event. Besides, the development of peculiar coronitic structures, which progressively substitute the domains of primary olivine (Tribuzio et al., 1997) with fibrous-radiate aggregates of chlorite and colourless amphiboles, sometimes associated to serpentine, was also observed. The amphiboles composition is generally tremolite or tremolite/actinolite (Messiga and Tribuzio, 1991; Riccardi et al., 1994). Both crenulation cleavage (Fig. 24) and narrow shear zones, millimetric/sub-millimetric in thickness, determining a microstructural recrystallization and located along the D_2 shear zones, are assigned to this event as well. Shear deformations and micro-faults, which determine a grain size reduction in the syn-D_2 amphiboles (and locally of plagioclase) and the syn-kinematic blastesis of green to colourless amphiboles (tremolite, actinolite) and of chlorite and serpentine, occasionally occur during the D_3 phase.

In the rock samples affected by D_3 recrystallizations, veins filled with associations of green to colourless amphiboles, with composition varying from tremolite to actinolite (Figs. 21 and 22, Table 3), were widely observed. Relations between the basalt dykes and the D_3 structures were instead never observed.

Cataclastic deformations

In the area of Pietra di Vasca, the mylonitic D_1 shear zones are associated to metric volumes of cataclasites (Fig. 25), characterized by angular to sub-angular millimetric to decimetric clasts in a matrix formed by monomineralic fragments of gabbro, with tremolite/actinolite + epidote + chlorite + Na-plagioclase. Some basalt dykes, reduced to a cataclastic assemblage of centimetric fragments, may also be associated to the cataclasites. Next to the cataclastic portions,

Fig. 25 - Cataclasites at Pietra di Vasca in gabbro.

the mylonitic shear zones in the gabbro may be deformed by open decimetric folds, with rounded hinges.

ORIENTATION AND AREAL DISTRIBUTION OF DEFORMATIONS

Regarding the analysis of internal geometry and orientation of structures of the BGC, one of the problems is the absence of guide stratigraphic levels, to serve as reference for unambiguous interpretation of the orientation of deformation. Magmatic layering can locally represent a reference level, yet often discontinuous and limited in extension. For these reasons the attitude of the pre-orogenic structures is here represented in different plots, each referred to areas where the outcropping rocks preserve original pre-orogenic structural continuity (Figs. 26 and 27).

All the study area is characterized by a distribution of

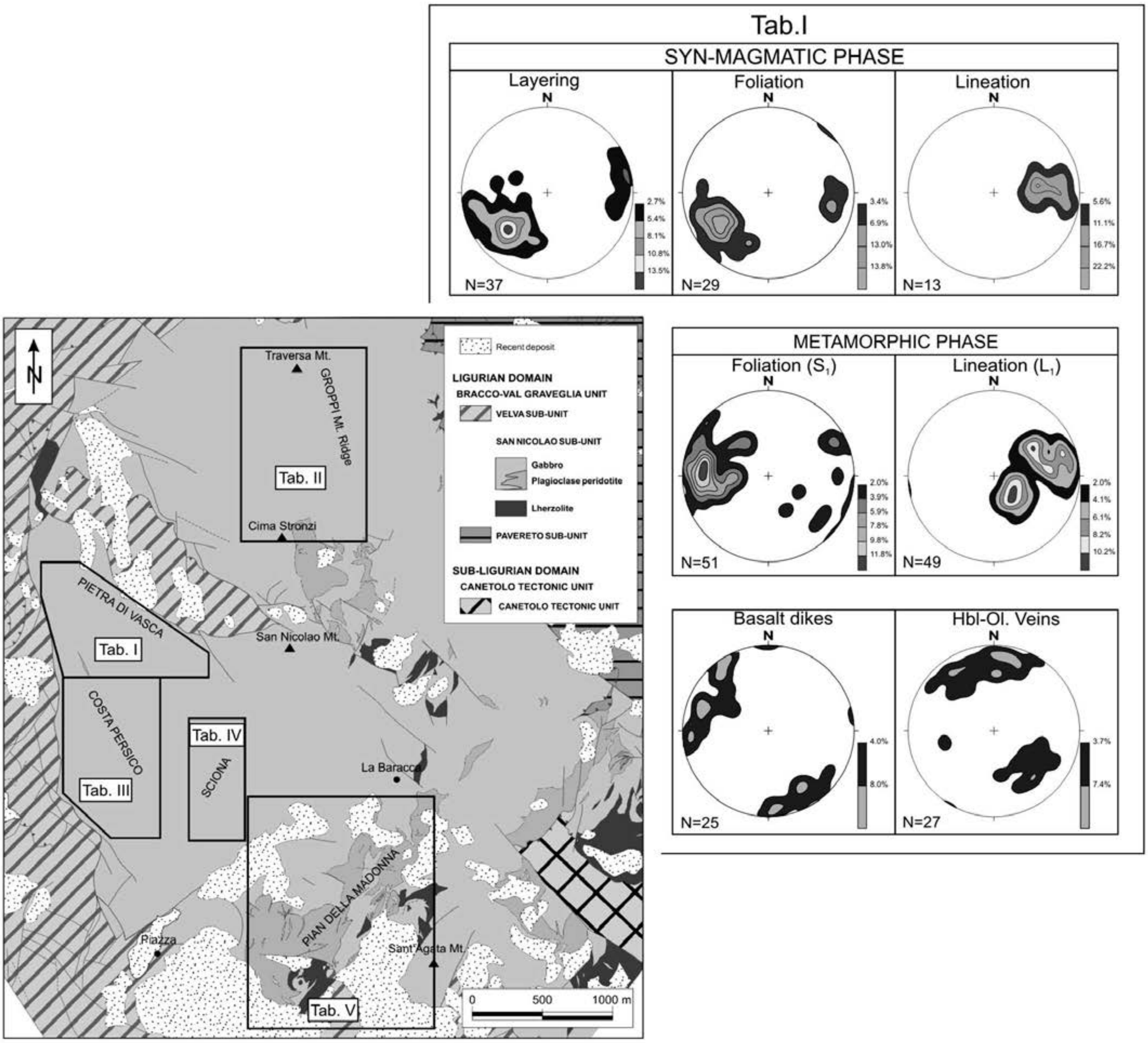

Fig. 26 - Stereographic projections of orientation of magmatic and metamorphic fabric elements for Pietra di Vasca area (Schmidt net, lower hemisphere, poles to foliation, layering, dykes and veins).

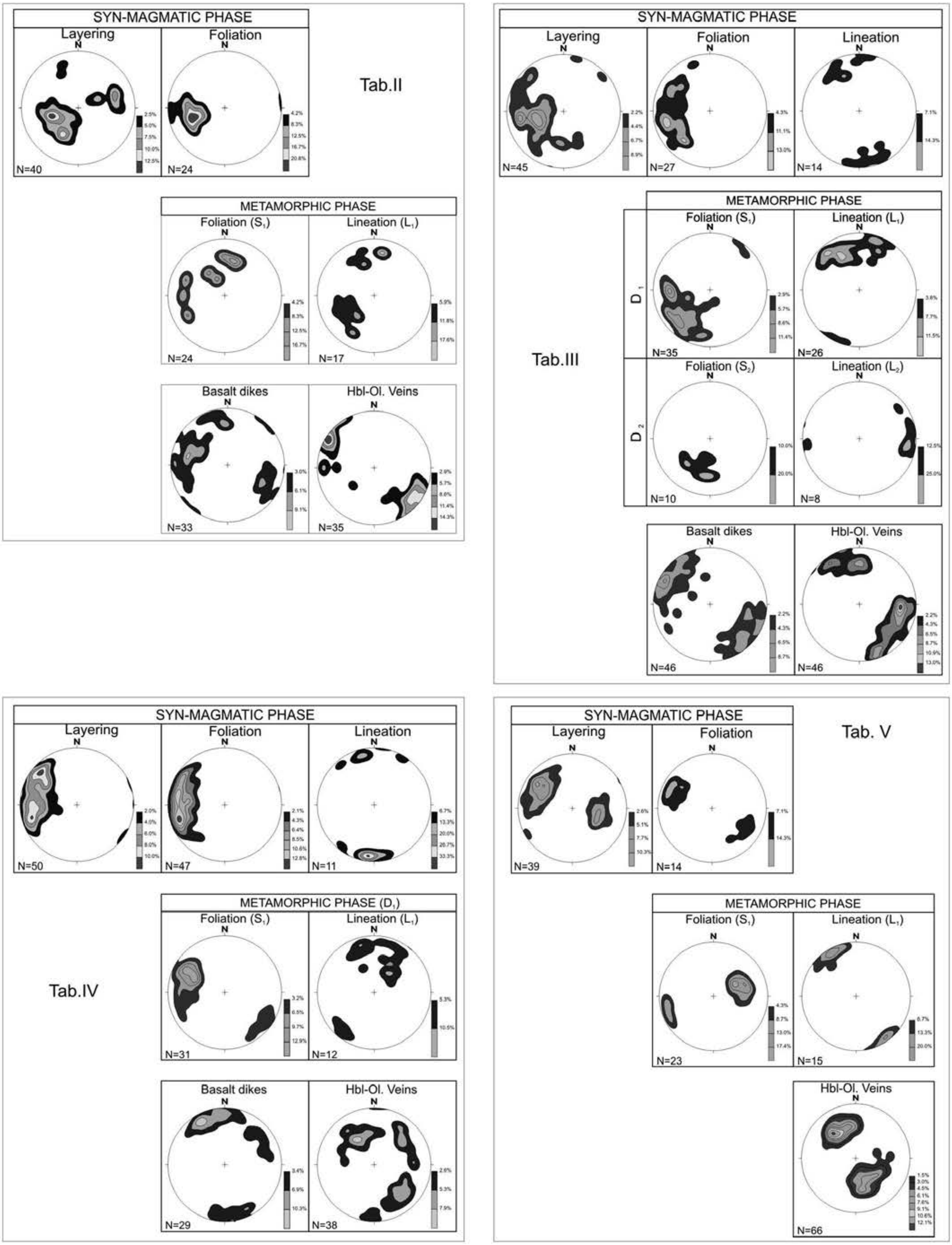

Fig. 27 - Stereographic projections of orientation of magmatic and metamorphic fabric elements for Mt. Groppi, Costa Persico, Sciona and Pian della Madonna areas (Schmidt net, lower hemisphere, poles to foliation, layering, dykes and veins).

layering and magmatic foliation generally oriented NW-SE or N-S and dipping toward E. Magmatic lineations instead show non uniform attitudes, with dipping directions varying from N-S to W. Metamorphic D_1 shear zones usually show a homogeneous orientation, typically dipping 50-80° towards E-NE, like the layering and the magmatic foliation. D_1 shear zones dipping at medium/high angles towards S or SE also occur. L_1 metamorphic lineations show fairly constant attitudes inside a shear zone, being however very scattered in the whole area. Based on their present orientation, the D_1 shear zones appear to be inverse, sometimes transcurrent, rarely normal.

Magmatic and metamorphic lineations are often parallel in the same volume of rock; in some narrow areas a congruent sense of shear can also be observed between the two.

D_2 shear zones are extremely rare and localized in narrow regions, located inside syn-D_1 shear zones. Rare S_2 surfaces usually dip about 10-30° towards N-NE; the L_2 lineations dip a few degrees towards E.

Basalt dykes and hornblende oligoclase veins are frequently associated and show a non-homogeneous distribution and variable attitudes in the study area. They are generally arranged in two families: one dipping toward NW and one toward E-SE, both about 50-70°. Nevertheless, in the Sciona region, these structures are generally oriented E-W, dipping about 60-80° both toward N and S.

DISCUSSION AND INTERPRETATION

For understanding the tectonics during the early genetic stages of the BGC, the most important features are the syn-magmatic structures represented by foliations, locally associated to lineations, folds and S-C shear zones. The presence of these fabric elements, often coupled with peculiar textural features, such as intracrystalline deformations, leads to exclude that the development of magmatic foliation could be due only to "compaction" or cumulus phenomena (Meurer and Boudreau, 1998), suggesting instead, at least for some sites, a viscous-laminar flow (Cannat, 1991; Nicolas, 1992; Gaggero and Cortesogno, 1997), probably characterizing a "crystal mush" and, later, its differentiates (Gaggero and Cortesogno, 1997). Moreover, because the magmatic foliation appears generally parallel to or slightly inclined with respect to the magmatic layering, the compositional (or granulometric) anisotropies can be considered parallel to the magma flow direction (Benn and Allard, 1989). This phenomenon, according to Nicolas (1992), could be due to the fact that the layering itself could work as an anisotropy and channel the flow parallel to itself. Nevertheless, where the magmatic foliation is not directly associated to lineations, folds, S-C shear zones and intracrystalline deformation, an origin by cumulus alone cannot be excluded.

After the magmatic phases, the BGC was characterized by deformations and mineralogic/petrographic riequilibrations under progressively decreasing metamorphic conditions (Fig. 28). The fabrics associated to the first metamorphic phase (D_1) are the most widespread, mainly corresponding to mylonitic shear zones with uniform attitude over large areas. From the petrographic point of view, the syn-kinematic recrystallization of diopsidic clinopyroxenes, associated to calcic plagioclases (An_{42-68}: Table 1) and locally to Ti-pargasite and ilmenite, generally occurs. Newly formed clinopyroxenes are characterized, with respect to the magmatic ones, by a loss in Al, associated to an increase in Ca, which indicates a sub-solidus magmatic origin, with temperatures lower than the primary ones during crystallization. TiO_2 content in the Ti-pargasites in association with neoblastic clinopyroxenes (Otten, 1983; Ernst and Liu, 1998) could suggest temperatures of 850-950°C (Tribuzio et al., 2000; Montanini et al., 2008). For the same mineralogic association Gaggero and Cortesogno (1997) propose slightly lower temperatures, comprised between 800°C and 900°C. The parageneses associated to this phase point to an evolution started in the granulitic facies and evolved towards conditions intermediate between the granulitic and the amphibolitic facies (Gaggero and Cortesogno, 1997).

The distribution of D_1 shear zones is frequently associated to magmatic layering and/or foliation and frequently parallel to them. Furthermore, congruence in vergence between the syn-magmatic and the D_1 metamorphic shear zones has been sporadically observed. Based on these observations, the D_1 phase could alternatively represent one of the two following tectonic scenarios:

1) a deformation event which followed the magmatic phase, but was genetically independent, although it took place under the same stress field as the one generating the syn-magmatic structures;
2) a deformation started in a magmatic context and continued in metamorphic conditions because of the diminishing melt percentage in the system. In this case, some of the fabrics observed in the gabbros and attributed to metamorphic phenomena (*Fabric I*), characterized by deformed, slightly recrystallized clinopyroxenes, could testify deformations that started inside a viscous magmatic flow and proceeded under a ductile regime ("*plastic flow or solid-state flow*"; Nicolas, 1992). Considering that the transitions between solid state deformations and viscous flow ones takes place gradually and that it depends on

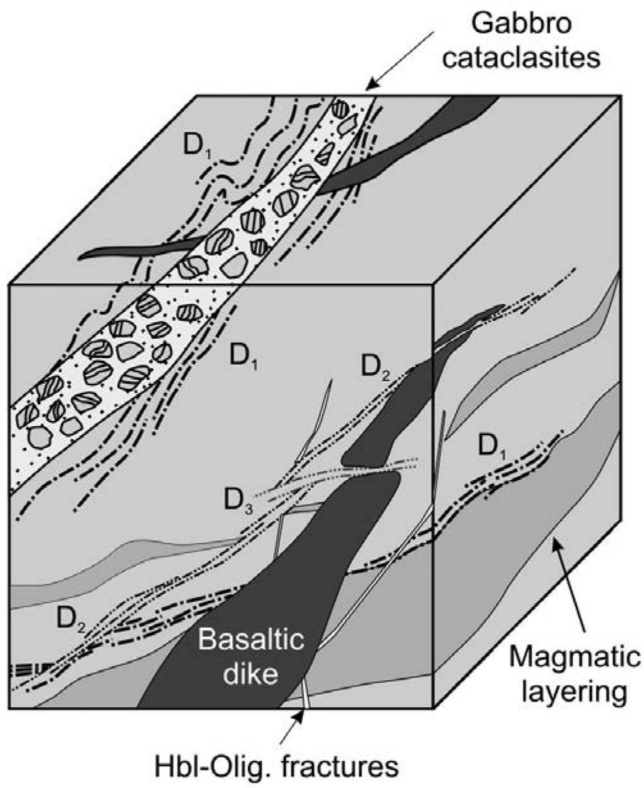

Fig. 28 - Schematic reconstruction summarizing superimposition relations between structures belonging to different deformation phases for the BGC.

the melt percentage in the system (Van der Molen and Paterson, 1979; Wickham, 1987; Nicolas, 1992), the development of the very first D_1 shear zones could have occurred in zones with very little melt fraction, contemporaneously to the formation of syn-magmatic structures, linked to viscous flow phenomena ("*viscous flow*": Nicolas, 1992) in other portions of the crystal mush, where a bigger liquid portion was present.

The second metamorphic phase M_2/D_2 developed at various scales in the studied gabbroic complex (Fig. 28). It rarely occurs as mesoscopic shear zones; more often, it is represented by deformations and/or recrystallizations at the petrographic/microstructural scale, such as the growth of amphiboles like Mg-hornblende (from brown to colourless) and edenite. The crystallization of brown Mg-hornblende in pressure tails around granoblastic assemblages of syn-D_1 clinopyroxenes, probably represents the transition between the first and the second deformation phase. The retrograde evolution of the latter is then responsible for the subsequent blastesis of Mg-hornblende from brown to green/colourless, as well as edenite. The first serpentinization phenomena probably took place during the very final moments of this phase, together with the crystallization of tremolitic amphiboles. The fragile structures, such as fractures/veins and the very first intrusion of basalt dykes, can be referred to the late parts of the M_2/D_2 phase. Cortesogno et al. (1994), on the basis of the coexistence of Mg-hornblende and edenite, attribute to analogous mineral associations in the gabbroic rocks of Liguria temperatures of about 550°C and pressures lower than 0.2 GPa. This metamorphic phase continued below 500°C (Shelley, 1993), as to include the beginning of serpentinization.

The last recognized metamorphic deformative phase D_3 (Fig. 28) is responsible for rare and narrow crenulations at the meso/microscale, locally dislocating the older structures, mainly associated to the blastesis of tremolite and actinolite under temperatures lower than 500°C.

The development of cataclasites could probably start during the second phase but it is well developed during the third phase, according both to the petrographic features and to the presence of basalt dykes involved in the cataclastic deformation (Fig. 28); their intrusion is believed to begin at the end of the second phase. The association of the cataclastic portions with the D_1 shear zones testifies that deformation started in a ductile regime and went on, or was reactivated in a fragile context, with lower P/T conditions. As stated by Molli (1992), we believe that the open folds which characterize the gabbro next to the cataclasites might be associated to "work hardening" (Molli, 1992) phenomena, linked to exhumation.

CONCLUSIONS

This study allowed to outline in detail a sequence of oceanic deformations that accompanied the evolution of a portion of oceanic lithosphere, the BGC, from the magmatic stage to its final uplift and exhumation on the oceanic floor. The results shed light on the genesis and tectonics of oceanic lithosphere in a low magma budget environment, where tectonics plays a major role in structuring oceanic crust and uplifting deep portions of oceanic lithosphere (oceanic core complex).

According to the collected data, some of the observed magmatic structures could be referred to the very early stages of the same deformation events, later responsible for the development of the first metamorphic structures in granulitic facies. In detail, the older structures in the gabbroic body, consist of magmatic layering and foliations, frequently associated to lineations and S-C shear zones, that demonstrate deformation occurring in syn-magmatic conditions. In the same way, some of the observed features suggest that the deformations attributed to the metamorphic phases could actually represent the evolution of the same metamorphic/deformation regime, that started under granulitic facies, continued in amphibolitic facies and ended with deformations and recrystallizations in greenschist facies.

The transition between granulitic and amphibolitic facies was likely due not only to a decrease in pressure and temperature conditions, but also to the input of seawater fluids in the system (Cortesogno et al., 1994, cum bibl.). Their circulation could have been favoured by the net of fractures which was starting to develop in the gabbro, possibly during the transition from ductile to fragile conditions, which likely began during the M_2/D_2 event or in its final part, together with the intrusion of basalts dykes.

In this work the classic subdivision in successive tectonic phases has been used for the analysis of petrographic and microstructural data. However, it is important to underline that these phases do not correspond to discrete tectono/metamorphic events, but to an evolution path, developed continuously in the BGC during its exhumation, from the very first magmatic phases until its final exposure on the Jurassic oceanic floor.

The entire evolution of the studied gabbroic complex, starting from its magmatic intrusion to the final uplift to the ocean floor, took place in a tectonically active oceanic environment. Some modern analogues can be found along several slow-spreading oceanic ridges (e.g., Atlantis Bank - Southwest Indian Ridge, Atlantis Massif - Mid-Atlantic Ridge), characterized by the exposure of "oceanic core complexes", or even along very slow spreading ridges (e.g., the Gakkel Ridge).

ACKNOWLEDGEMENTS

Francesca Garfagnoli, Benedetta Treves and Gianfranco Principi are thanked for reading the manuscript and for the stimulating discussions.

REFERENCES

Abbate E. and Sagri M., 1970. The eugeosynclinal sequences. In: G. Sestini (Ed.), Development of the Northern Apennines geosyncline. Sedim. Geol., 4 (3/4): 251-340.

Beccaluva L., Macciotta G., Piccardo and Zeda O., 1984. Petrology of lherzolitic rocks from Northern Apennine ophiolites. Lithos, 17: 299-316.

Bell T.H. and Etheridge M.A., 1973. Microstructure of mylonites and their descriptive terminology. Lithos, 6: 337-348.

Benn K. and Allard B., 1989. Preferred mineral orientations related to magmatic flow in ophiolite layered gabbros. J. Petrol., 30: 925-946.

Berthé D., Choukroune P. and Gapais D., 1979a. Orientations préférentielles du quartz et orthogneissification progressive en régime cisaillant: l'exemple du cisaillement sud-armoricain. Bull. Minéral., 102: 265-272.

Berthé D., Choukroune P. and Jegouzo P., 1979b. Orthogneiss, mylonite and non-coaxial deformation of granites: the example of the South Armoricain shear zone. J. Struct. Geol., 1: 31-42.

Bezzi A. and Piccardo G.B., 1971. Structural features of the Ligurian ophiolites: petrologic evidence for the oceanic floor of the Northern Apennines geosyncline; a contribution to the problem of the alpinotype gabbro-peridotite associations. Mem. Soc. Geol. It., 10: 53-63.

Cannat M., 1991. Plastic deformation at an oceanic spreading ridge: a microstructural study of Site 735 gabbros (southwest Indian Ocean). In: R. Von Herzen, P.T. Robinson et al. (Eds.), Proc. ODP, Sci. Results, 118: 399-408. DOI:10.2973/odp.proc.sr.118.134.1991.

Cortesogno L. and Gaggero L., 1992. The basaltic dikes in the Bracco gabbroic massif: petrology of the earliest phases of basaltic activity in the Northern Apennines Ophiolites. Ofioliti, 17 (2): 183-198.

Cortesogno L., Gaggero L. and Molli G., 1994. Ocean floor tectono-metamorphic evolution in the Piedmont-Ligurian Jurassic basin: a review. Mem. Soc. Geol. It. 48: 151-163.

Cortesogno L., Galbiati B. and Principi G., 1987. Note alla "Carta geologica delle ofioliti del Bracco" e ricostruzione della paleogeografia Giurassico-Cretacica. Ofioliti, 12: 261-342.

Cortesogno L., Gianelli G. and Piccardo G.B., 1975. Pre-orogenic metamorphic and tectonic evolution of the ophiolite mafic rocks (Northern Apennine and Tuscany). Boll. Soc. Geol. It., 94: 291-321.

Cottin J.Y., 1978. L'association ultramafique-mafique de la région du Bracco (Apennin Ligure, Italie). Thèse Doct., Univ. Paris VII.

Decandia F.A. and Elter P., 1972. La zona ofiolitifera del Bracco nel settore compreso tra Levanto e la Val Graveglia (Appennino Ligure). Mem. Soc. Geol. It., 11: 503-530.

Ernst W.G. and Liu J., 1998. Experimental phase-equilibrium study of Al- and Ti-contents of calcic amphibole in MORB-A semiquantitative thermobarometer. Am. Mineral., 83: 952-969.

Gaggero L. and Cortesogno L., 1997. Metamorphic evolution of oceanic gabbros: recrystallization from subsolidus to hydrothermal conditions in the MARK area (ODP Leg 153). Lithos, 40 (2\4): 105-131.

Garuti G., Alfonso P., Proenza J. A. and Zaccarini F., 2009. Sulfur-isotope variations in sulfide minerals from massive sulfide deposits of the Northern Apennine ophiolites: inorganic and biogenic constraints. Ofioliti, 34 (1): 43-62.

Gianelli G. and Prncipi G., 1974. Studies on mafic and ultramafic rocks. 4 - Breccias of the ophiolitic suite in the Monte Bocco area (Ligurian Apennine). Boll. Soc. Geol. It., 93: 277-308.

Hanmer S. and Passchier C.W., 1991. Shear sense indicators: a review. Geol. Surv. Can., 90, 72 pp.

Hobbs B.E., Means W.D. and Williams P.F., 1976. An outline of structural geology. Wiley, New York, 571 pp.

Hoogerduijn-Strating E.H., 1988. High temperature shear zones in the gabbroic massif (N. Apennines, Italy): possible implications for tectonic models of ocean floor generation. Ofioliti, 13 (2\3): 111-126.

Hoogerduijn-Strating E.H., 1991. The evolution of the Piemonte-Ligurian ocean, a structural study of the ophiolite complexes in Liguria (NW Italy). PhD Dissert., Utrecht Univ., 127 pp.

Hoogerduijn Strating E.H., Rampone E., Piccardo G.B., Drury M.R. and Vissers R.L.M., 1993. Subsolidus emplacement of mantle peridotites during incipient oceanic rifting and opening of the Mesozoic Tethys (Voltri Massif, NW, Italy). J. Petrol., 34: 901-927.

Kretz R., 1983. Symbols for rock-forming minerals. Am. Mineral., 69: 277-279.

Krohe A., 1990. Local variations in quartz (c)-axis orientations in non-coaxial regimes and their significance for the mechanism of S-C fabrics. J. Struct. Geol., 12: 995-1004.

Leake B.E., Wooley A.R., Arps C.E.S., Birch. W.D. Gilbert M.C., Grice J.D., Hawthorne F.C., Kato A., Kisch H.J., Krivivichev V.G., Linthout K., Laird J., Mandarino J.A., Maresch W.V., Nickel E. H., Rock N.M.S., Schumacher J.C., Smith D.C., Stephenson N.C.N., Ungaretti L., Whittaker E. and Youzhi G., 1997. Nomenclature of amphiboles: report of the subcommittee on amphiboles of the International Mineralogical Association, commission on New Minerals and Minerals Names. Can. Mineral., 35: 219-246.

Lister G.S. and Snoke A.W, 1984. S-C Mylonites. J. Struct. Geol., 6: 617-638.

Messiga B. and Tribuzio R. 1991. Steady mineral sequence generated by reaction between olivine and plagioclase during subseafloor metamorphism in Al-Mg gabbros, Northern Apennine ophiolites, Italy. Ofioliti, 16 (1): 7-15.

Meurer W.P. and Boudreau A.E., 1998. Compaction of igneous cumulates. Part II: Compaction and the development of igneous foliations. J. Geol., 106: 293-304.

Molli G., 1992. Evoluzione strutturale di shear zones nel complesso gabbrico del Bracco (Appennino Settentrionale). Atti Ticinesi. Sci. Terra, 35: 19-23.

Molli G., 1994. Microstructural features of high temperatures shear zones in gabbro of the Northern Apennine ophiolites. J. Struct. Geol., 16: 1535-1541.

Molli G., 1995. Pre-orogenic high temperature shear zones in an ophiolite complex (Bracco Massif, Northen Apennine, Italy). In: R.L.M. Visser and A. Nicolas (Eds.), Mantle and lower crust exposed in oceanics ridges and ophiolites, Kluwer Academic Publishers, p. 146-161.

Molli G., 1996. Pre-orogenic tectonic framework of the northern Apennine ophiolites. Ecl. Geol. Helv., 89 (1): 163-180.

Montanini A., Tribuzio R. and Vernia L., 2008. Petrogenesis of basalts and gabbros from an ancient continent-ocean transition (External Liguride ophiolites, Northern Italy). Lithos, 101: 453-479.

Morimoto N., Fabires J., Ferguson A.K., Ginzburg I.V., Ross M., Seifert F.A., Zussman J., Aoki K. and Gottardi G., 1988. Nomenclature of pyroxenes. Am. Mineral., 73: 1123-1133.

Nicolas A., 1987. Principles of rock deformation. D. Reidel, Dordrecht, 208 pp.

Nicolas A., 1989. Structures of ophiolites and dynamics of oceanic lithosphere. Kluwer, Dordrecht, 367 pp.

Nicolas A., 1992. Kinematics in magmatic rocks with special reference to gabbro. J. Petrol., 33 (4): 891-915.

Otten M.T., 1983. The origin of brown hornblende in the Artfjället gabbro and dolerites. Contr. Mineral. Petrol., 86:189-199.

Passchier C.W. and Simpson C., 1986. Porfiroclast systems as kinematic indicators. J. Struct. Geol., 8: 831-844.

Passchier C.W. and Trouw R.A.J., 1996. Microtectonics. Springer-Verlag, Berlin Heidelberg, 2nd corrected reprint, 289 pp.

Passerini P., 1965. Rapporti fra le ofioliti e le formazioni sedimentarie fra Piacenza e il Mare Tirreno. Boll. Soc. Geol. It., 84 (5): 93-176.

Paterson S.R., Vernon R.H. and Tobisch O.T., 1989. A review of criteria for the identification of magmatic and tectonic foliations in granitoids. J. Struct. Geol., 11: 249-363.

Piccardo G.B., Rampone E. and Vannucci R., 1990. Upper mantle evolution during continental rifting and ocean formation: evidence from peridotite bodies of the Western Alpine - Northern Apennine system. Mém. Soc. Géol. Fr., 156: 323-333.

Piccardo G.B., Rampone E., Vannucci R. and Cimmino F., 1994. Upper mantle evolution of ophiolitic peridotites from the Northern Apennines: petrological constraints of the Geodynamic processes. Mem. Soc. Geol. It., 48: 137-148.

Principi G., Bortolotti V., Chiari M., Cortesogno L., Gaggero L., Marcucci M., Saccani E. and Treves B., 2004. The pre-orogenic volcano-sedimentary covers of the western Tethys oceanic basin: a review. Ofioliti, 29 (2): 177-211.

Rampone E. and Piccardo G.B., 2000. The ophiolite - oceanic lithosphere analogue: new insights from the Northern Apennine (Italy). In: Y. Dilek, E. Moores, D. Elthon and A .Nicolas (Eds.), Ophiolites and oceanic crust: new insights from field studies and Ocean Drilling Program. Am. Geol. Soc. Spec. Paper, 349: 21-34.

Rampone E., Piccardo G.B., Vannucci R., Bottazzi P. and Ottolini L., 1993. Subsolidus reactions monitored by trace element partitioning: the spinel- to plagioclase-facies transition in mantle peridotites. Contrib. Mineral. Petrol., 115: 1-17.

Ramsay J.G. and Graham R.H., 1970. Strain variation in shear belts. Can. J. Earth Sci., 7: 786-813.

Riccardi M.P., Tribuzio R. and Cauccia F., 1994. Amphibole evolution in the metagabbros from East Ligurian ophiolithes (Northern Apennines, Italy): constraints on the ocean-floor metamorphism. Mem. Soc. Geol. It., 48: 203-208.

Shelley D., 1993. Igneous and metamorphic rocks under the microscope. Classification, textures, microstructures and mineral preferred orientaions. Chapman and Hall, London, 445 pp.

Simpson C. and Schmidt S.M., 1983. An evaluation of criteria to determine the sense of movement in sheared rocks. Bull. Geol. Soc. Am., 94: 1281-1288.

Treves B. and Harper G.D., 1994: Exposure of serpentinites on the ocean floor: sequence of faulting and hydrofracturing in the Northern Apennine ophicalcites. Ofioliti, 19: 435-466.

Tribuzio R., Riccardi M.P. and Messiga B., 1997. Amphibolitization of Mg-and Fe-rich gabbroic dykes within mantle-derived serpentinites from Northern Apennine ophiolites: evidence for high-temperature hydration of the oceanic lithosphere. Ofioliti, 22: 71-80.

Tribuzio R., Tiepolo M. and Vannucci R., 2000. Evolution of gabbroic rocks from the Northern Apennine ophiolites (Italy): comparison with the lower oceanic crust from modern slow-spreading ridges. In: Y. Dilek, E. Moores, D. Elthon, and A. Nicolas (Eds), Ophiolites and oceanic crust: New insights from field studies and Ocean Drilling Program. Geol. Soc. Am., Spec. Paper, 349: 129-138.

Tullis J.T., Snoke A.W. and Todd V.R., 1982. Significance of petrogenesis of mylonitic rocks. Geology, 10: 227-230.

Van der Molen I. and Paterson M.S., 1979. Experimental deformation of partially-melted granite. Contr. Miner. Petrol., 70: 299-318.

Vernon R.H., Williams V.A. and D'Arcy W.F., 1983. Grain-size reduction and foliation development in a deformed granitoid batholith. Tectonophysics, 92: 123-145.

White S.H., Burrows S.E., Carreras J., Shaw N.D. and Humphreys F.J., 1980. On mylonites in ductile shear zones. J. Struct. Geol., 2: 175-187.

Wickham S.M., 1987. The segregation and emplacement of granitic magmas. J. Geol. Soc. London, 144: 281-297.

Received, June 16, 2009
Accepted, December 2, 2009